AD NUMBER

AD482809

LIMITATION CHANGES

TO:

Approved for public release; distribution is unlimited.

FROM:

Distribution authorized to U.S. Gov't. agencies and their contractors; Critical Technology; 1961. Other requests shall be referred to U.S. Naval Postgraduate School, Monterey, CA 93943. This document contains export-controlled technical data.

AUTHORITY

USNPS ltr, 23 Sep 1971

THE INSTALLATION AND PERFORMANCE EVALUATION OF A SMALL SUPERSONIC WIND TUNNEL SYSTEM

CHARLES O. BROWN

THE INSTALLATION AND PERFORMANCE EVALUATION OF A SMALL SUPERSONIC WIND TUNNEL SYSTEM

****

Charles O. Brown

THE INSTALLATION AND PERFORMANCE EVALUATION OF A SMALL SUPERSONIC WIND TUNNEL SYSTEM

by

Charles O. Brown

Lieutenant Commander

United States Navy

Submitted in partial fulfillment of
the requirements for the degree of

MASTER OF SCIENCE
IN
MECHANICAL ENGINEERING

United States Naval Postgraduate School
Monterey, California

1961

THE INSTALLATION AND PERFORMANCE EVALUATION OF A SMALL SUPERSONIC WIND TUNNEL SYSTEM

by

Charles O. Brown

This work is accepted as fulfilling
the thesis requirements for the degree of
MASTER OF SCIENCE
IN
MECHANICAL ENGINEERING
from the
United States Naval Postgraduate School

TABLE OF CONTENTS

ABSTRACT

This report describes the procedure utilized in the assembly and evaluation of a small intermittent blowdown supersonic wind tunnel.

The tunnel proper was fully constructed and nozzle blocks for attainment of a Mach number of 1.5 or 2.37 in the 1/2" by 1.718" test section were available. The basic schlieren system was purchased complete. An attempt was made to use or convert readily available materials for all components.

It was expected the results of this project would be of a permanent nature and would be utilized by the Mechanical Engineering Department as a laboratory installation. The installation is suitable for the study of compressible fluid flow and the phenonemon of normal shocks but is not suitable for the study of the performance of shapes or models in the fluid flow.

The tunnel installation operates satisfactorily with a maximum Mach number of 2.29 with approximately 0.28 lbm of air per second. Schlieren photographs of the flow field may be taken in either black and white or in color.

ACKNOWLEDGEMENT

The author wishes to express his appreciation to Professor Charles P. Howard for his guidance, assistance and numerous benefical suggestions during all phases of the project. Appreciation is also extended to Messrs. K. W. Mothersell and Joseph Beck for their assistance in the construction and installation of the tunnel components.

LIST OF ILLUSTRATIONS

LIST OF TABLES

LIST OF SYMBOLS

α	Acute Angle between Mach Wavelet and horizontal line, degrees
A	Area, sq. in.
A^*	Area in tunnel where M = 1.00, sq. in.
A_x^*	Area in tunnel upstream of shock where M = 1.00, sq. in.
A_y^*	Area in tunnel downstream of shock where M = 1.00, sq. in.
C_D	Coefficient of discharge
$\dot{m}$	Mass rate of flow - lbm/sec.
P	Tunnel pressure, in. Hg.a.
ΔP	Differential between stagnation pressure and tunnel pressure, in. Hg.
ΔP_{orf}	Differential pressure across orifice plate, inches of water
P_{ob}	Tunnel back pressure, in. Hg.a.
P_{on}	Stagnation pressure of any point n downstream of shocking system, in. Hg. a.
P_{ol}	Stilling tank stagnation pressure, in. Hg. a.
P_{ox}	Stagnation pressure upstream of shock, in. Hg.a.
P_{oy}	Stagnation pressure downstream of shock, in. hg.a.
T	Local temperature, ^oR
T_{ol}	Stilling tank stagnation temperature, ^oR

INTRODUCTION

There are two basic types of wind tunnels available for the study of compressible fluid flow (1) the continuous and (2) the intermittent, [11] *. With continuous wind tunnels the problem of matching compressor, tunnel volume flow and pressure ratio characteristics present major difficulties in the design work. In addition the Mach number span of a continuous wind tunnel is usually small and does not extend from low subsonic velocities to high supersonic velocities. These factors combined with a higher cost of installation and operation of the continuous tunnel have resulted in a shift towards the use of the intermittent tunnels.

The intermittent tunnel is further divided into two basic types (1) the vacuum storage drive and (2) the pressure storage drive, [11] . In the first system, atmospheric air passes through a drier, wind tunnel and diffuses into a vacuum vessel which is continuously evacuated to the atmosphere. In the second system, dry air is stored under pressure in a storage tank; the air passes through a throttle valve, wind tunnel and exhausts through a tunnel diffuser to the atmosphere.

It was the objective of this thesis to install and evaluate the performance of a small pressure storage type supersonic wind tunnel system. The components available at the start of the project consisted of: high pressure compressor; storage tanks; two regulator valves; tunnel test section; and Schlieren system components; all other pieces for the system had to be either specified or designed and specially constructed. It was further necessary to carry out assembly and installation of these components. Having completed this phase of the objective, it was then

* Numbers in brackets refer to the Bibliography on page 20.

possible to undertake a performance evaluation program. This consisted of both a qualitative and an quantative approach. The qualitative evaluation was derived primarily from Schlieren photographs, while the quantitative results came primarily from pressure surveys.

Figure 1 is a schematic diagram of the system showing the basic design and necessary components. Discussion of the design and pertinent details of certain sections of the system is found in Part I.

Figure 2 is a subassembly drawing of the small tunnel test section for which the performance tests were made. Results of these tests are presented in photographs, graphical form, and tabular form. Discussion of these tests and results appear in Part II.

The Appendicies include various sample calculations, a discussion of Schlieren systems, operational instructions, design of a differential pressure transducer, and design of needed heat capacitors for the air receivers.

Part I. Tunnel System Design

A. Air Supply.

Air for the system was supplied by a Chicago Pneumatic two stage inner cooled air compressor rated at 114 cubic feet of free air per minute or 0.142 pounds per second. The compressor is driven by a 50 horsepower induction electric motor. The compressor discharge pressure can be controlled up to 500 psi by the regulator valve (Bailey Type-XSDS-9M). Operational instructions for the compressor are given in Appendix A.

Air from the compressor goes to an after-cooler (Graham Heliflow, Type 9AA 145) where the temperature is reduced to about 60°F, and then to a cyclone type separator with trap (Wright Austin), where the condensed water is removed. Calculations show the moisure content after the air leaves the separator to be about 0.000319 lb. water per lb of dry air, Appendix B. Drying of the air is necessary to prevent condensation from occuring in the tunnel test section, [6], [11], [12].

From the separator, the air passes through an oil filter (C. M. Kemp, Type FPF-1610), using activated alumina (Vapoilsorb) as a desiccant. This filter was modified by putting a 60 mesh stainless steel strainer on the inlet side along with a fiberpacked strainer. This modification was made to prevent blowback of desiccant particles to the compressor by high pressure air when the compressor was unloaded.

The air then goes through the regulator valve, which maintains a constant compressor discharge pressure, to the two air receivers. The receivers, connected in parallel, provide a total storage volume of 234 cubic feet. Figure 3 is a photograph showing these various components in relation to the acoustic enclosure which houses the compressor.

When operating the wind tunnel, the mass flow of air from the receivers to the tunnel section is controlled by a regulator valve (Bailey, Type XSDS-9M). The regulator valve provides for stagnation pressure control up to 200 psi. Figure 4 shows the position and location of this valve.

B. Tunnel Section.

The tunnel section consists of six basic parts: stilling tank; entrance nozzle; test section; diffuser; flow meter; and back pressure control.

The stilling tank was made from a 30 inch piece of nominal 6 inch pipe flanged at both ends. The flanges were faced and grooved for use with O-ring seals. The upstream end of the tank was connected by means of a piece of high pressure rubber hose to the regulator valve discharge. Figure 5 is a photograph of these pieces. In the upstream end of the stilling tank, 3 stainless steel 60 mesh screens were used to diffuse any high velocity profile.

The entrance nozzle was constructed of a polyester resin and chopped fiber glass molded over a wooden core. A pair of cubic equations were used to define the nozzle contour so that flow separation would not occur. The flanges were molded integral with the nozzle and were faced and drilled after casting. The upstream flange has a 1/2 inch lip for a matching connection with the stilling tank.

The test section was designed and constructed by the Ames Aeronautical Laboratory, Moffett Field, California. Features of this test section consist of a variable area supersonic diffuser, interchangeable nozzle blocks, and interchangeable side walls for either visual or pressure surveys.

The present sets of nozzle blocks are for Mach numbers 1.50 and 2.37. The sidewall for pressure surveys is provided with 32 pressure taps. Figure 2 is a subassembly drawing of the section and Figure 6 is a photograph showing the section with side walls removed. Tables I and II give the nozzle coordinates, area ratios, and design Mach numbers and pressure ratios based on one-dimensional calculations for the two sets of nozzle blocks.

The diffuser, like the entrance nozzle, was also molded over a wooden core with a polyester resin and fiber glass. To provide added strength, 1/8 by 3/8 inch steel bars were molded into the side and flanges. The design was strafght wall with a maximum divergance angle of 7° to prevent flow separation; and diffusion of the air stream was carried to a point where the flow could be treated as incompressible for metering purposes.

The four pieces just described were integrally mounted to a movable stand and are shown in Figure 7.

The flow meter was designed according to A.S.M.E. standards for a sharp edge orifice with D and (1/2)D pressure taps, [4] , [5] . An entrance length of 20 pipe diameters and an exit length of 10 pipe diameters were provided. Nominal 3 inch pipe was used which was bored to a 3.120 inch diameter for 16 inches either side of the orifice. O-ring seals were used throughout including the flanged joint with the diffuser. Orifice plates were made of 1/8 inch stainless steel. Appendix C presents the details for computing mass flow rates.

The back pressure control consisted of a manually operated 3 inch globe valve. This control was incorporated so that changes could be made

in the test section air density. Since this throttling was somewhat noisy, a large truck muffler was added to the valve exit.

These pieces were also mounted on a movable stand and are shown in Figure 8.

The completely assembled tunnel section is shown in the photograph, Figure 9.

C. Instrumentation.

Instrumentation for the tunnel section consisted of devices for three types of measurement; pressure, temperature, and velocity.

Manometers were used for all quantitative pressure measurements while bourdon tube gages were used for qualitative check purposes. Two 120 inch mercury differential manometers were utilized with the 32 tap pressure survey sidewall of the test section. Two 16 connector manifolds with quick opening valves were made to accommodate the 32 taps to the two manometers. Figure 10 shows the arrangement of the manifolds with the manometers. It was originally planned to produce strain gage type differential pressure transducers for these measurements to decrease the reading time required; fabrication difficulties, however, prevented the completion of this project, Appendix D.

A 120 inch mercury differential manometer was also used to monitor the test section throat pressure continuously during pressure survey runs.

Stagnation pressure, from the stilling tank tap, was likewise continuously monitored with a 120 inch mercury manometer besides being fed to the differential manometers.

Static pressure for the flow meter could be read with either an oil (sp. gr. = 0.834) or mercury filled 60 inch manometer. Differential pressure for the orifice was determined with a water manometer.

Ellison inclined manometers were used in conjunction with the pitot tube.

The only quantitative temperature measured was the stagnation temperature in the stilling tank. This was accomplished with a stainless steel radiation shielded 30 gage copper-constantan thermocouple referenced to ice. The output emf of the thermocouple was read with a continuous balance precision potentiometer (Minneapolis-Honeywell, Model SY156X-VH). Various other temperatures of the tunnel system were measured with gas bulb indicating thermometers.

Velocity measurements in the stilling tank were made with a 1/8 inch diameter Prandtl-Pitot probe. These measurements were made solely for the purpose of determining the uniformity of the velocity profile leaving the straightening screens in the stilling tank and were only of a qualitative nature. The Pitot probe was removed from the stilling tank after finding that the screens adequately diffused the high velocity entering air to a uniform low velocity profile.

Velocity measurements and visual flow studies in the test section were accomplished with a coincidence type Schlieren system manufactured by Tinsley Laboratories Inc. A schematic diagram is shown in Figure 11. The components were mounted to a rigid moveable stand with the wheels set in tracks parallel to the test section, Figure 8. The viewing section of the Schlieren system was modified by installation of an Ilex Synchro shutter and a 4 by 5 inch ground glass view plate and film pack holder, Figure 12. This modification allowed photographs of the flow behavior to be made which, when enlarged in printing, provided for qualitative and some quantitative measurements. Appendix E

presents a general theory of the Schlieren method of flow visualization as well as operating instructions for this particular system.

Part II. Performance Evaluation

A. Qualitative Results.

The qualitative evaluation of the tunnel system performance was derived primarily from Schlieren photographs. Figure 13 depicts the tunnel section operation under shock free conditions. The knife edge intercepted the light beam in both a vertical and horizontal position to show the change of density patterns in the horizontal and vertical directions. Figure 13c, with the knife edge horizontal, clearly shows the boundary layer.

Criss-crossing the tunnel outline are Mach wavelets produced by wall friction and other irregularities of the tunnel surfaces. These wavelets are related [2] to the Mach number of the air flow in the tunnel by the relationship,

$$\sin \alpha = \frac{1}{M}$$

where α is the acute angle between the wavelets and a horizontal line. Figure 18a is an enlargement of a section of Figure 13a and Figure 18b is an enlargement of Figure 13b. The angle α in Figure 18a is 27.50° with a resulting Mach number of 2.17. This wavelet originated at the junction of the nozzle and the test section. Utilizing the pressure ratios, the Mach number at the corresponding point was determined to be 2.125. The angle α in Figure 18b is 29.25° with a resulting Mach number of 2.04. The Mach number calculated for this position was 1.828. This wavelet originated at approximately pressure tap 30.

Figure 14 depicts a normal shock occuring in the diffuser section which was being held at a constant height of 1.718 inches. Inner action between the shock and the boundary layer is clearly indicated. Upstream of the shock the boundary layer is stable. At station 12 there

is a separation of the boundary layer due to the interaction of the shock and the boundary layer. Less severe interaction occurs between the boundary layer and the repeated shocks downstream until complete subsonic flow is established downstream of station 15.

Comparing Figure 14a operating under a stagnation pressure of 67 inches of mercury and a back pressure of 30.5 inches of mercury to Figure 14c for tunnel operation with a stagnation pressure of 81.5 inches of mercury and a back pressure of 38.3 inches of mercury, it may be seen that the resultant shock has moved upstream almost three inches. The pressure ratio at station 11 in Figure 14a where no shock exists is approximately 0.1088 as taken from Figure 23 or Table V. At a point forward of the shock in Figure 14c a pressure ratio of 0.103 exists as taken from Table VII.The increased density of the air and the higher Reynolds number must account for the shock moving upstream.

Reduction of the stagnation pressure also moves the shock upstream as shown in the sequence of photographs in Figure 15. A strong shock exists at the nozzle exit of Figure 15a with a stagnation pressure of 65.35 inches of mercury. Reduction of the stagnation pressure to 59.96 inches of mercury allowed the shock to move upstream one and one half inches towards the nozzle throat as shown in Figure 15c. Reduction of the shock intensity may be noted also as the shock moves upstream by comparing Figures 15a and 15c.

The minimum starting area of the variable diffuser was found to range between 0.695 and 0.700 square inches as compared to the isentropic minimum area of 0.665 square inches. The area actually required corresponds to a diffuser heights of 1.39 to 1.40 inches. Figure 16a is a photograph of the diffuser nozzle set at a height of 1.39 inches. The

shock could not be blown through the diffuser with a stagnation pressure of 82.71 inches of mercury. Increasing the diffuser height to 1.40 inches, (area change of 0.005 square inches) permitted the shock to be blown through the diffuser nozzle and the stagnation pressure reduced as shown in Figure 16b. The stagnation pressure could have been reduced to move the shock farther upstream to the throat position. Figure 17a and 17b depict tunnel operation with the diffuser height set slightly greater than the required minimum and show the shock standing in the diffuser throat and the stagnation pressure reduced to a minimum while maintaining the shock location. Several minutes after Figure 17a was taken the stagnation pressure was reduced from 60.00 inches of mercury to 59.50 inches of mercury and the shock moved through the diffuser nozzle and relocated itself in the diverging portion of the tunnel nozzle.

The sharpness of the Schlieren photographs was poor due to the use of non-collimated light and the fact the light beam passed through the test region twice, Appendix E. Figure 16c gives an indication of the seriousness of this problem. The knife edge was not inserted into the light beam. The black parallel vertical lines are images produced by placing fine copper wires on the outside of the Schlieren window nearest to the spherical mirror; the diagonal parallel lines are images produced by placing the same size wire on the outside of the Schlieren window nearest to the light source. The greater the distance between the images of any wire, the farther the light beam had to travel before reaching the spherical mirror. The non-parallel light beam intercepted the diagonal wire first and hence the image of this wire was deflected more due to the longer distance to the spherical mirror than it was for

any of the vertical wires which were closer to the spherical mirror. As evidenced by the two images formed for each wire, the Schlieren picture of the of the air flow would tend to be fuzzy due to superimposing the two images formed. The horizontal black line is a wire placed at the tunnel centerline.

Also contributing to poor quality of the Schlieren pictures was the incomplete removal of oil vapor from the air. During tunnel operation, oil would be deposited in a very thin film on the glass wall and cause a refraction of the light. In addition, the film deposited was not of a uniform nature. This condition may be seen in Figure 17c. The dark convex lines at stations 4 and 5 are the result of an oil film deposit. These same lines could still be seen after securing the air supply and leaving the Schlieren unit in operation. Due to this oil film formation, it was necessary to remove the Schlieren window at frequent intervals and wipe off the small amount of oil that had been deposited. Water vapor in the atmosphere condensing on the outside surface of the Schlieren window was also a factor in obtaining clear Schlieren photographs.

As the vertical wires were spaced at one inch intervals, the distance between wires in the photograph may be measured and comparison of this measured value to the known one inch dimension permits determining a scale factor for the photograph. This method was utilized to determine the diffuser heights for heights other than 1.718 inches. A lucite gage block, 1.718 inches high, was utilized when runs of this diffuser height were made.

The apparent difference in intensity of the shock and the visibility of the boundary layer caused by the knife edge orientation demonstrates why a horizontal knife is generally used when studying boundary layers and a vertical knife is used when studying shock waves.

B. Quantitative Results.

The quantitative evaluation was derived primarily from pressure surveys. The Mach numbers actually obtained in the tunnel were generally less than the predicted adiabatic Mach numbers due to friction effects not accounted for, oblique shocks and other departures from a one dimensional flow analysis. Figure 20 is a plot of the adiabatic Mach numbers obtained from the pressure and area ratios for a constant diffuser height of 1.718 inches vs. distance downstream of the tunnel nozzle throat. The solid curve is the isentropic Mach number based on the change of area ratios only as given in Table I, while the dashed curve is the predicted adiabatic curve as determined by the use of isoclines in Appendix F. The circles are the adiabatic Mach numbers obtained from the data taken on the tunnel and are tabulated in Table V, based on the procedure outlined in Appendix F.

Up to a Mach number of 1.936 at pressure tap number 4, the actual Mach numbers followed the adiabatic curve closely, exceeding both the isentropic and adiabatic curves between pressure taps numbers 4 and 7. At this point, the Mach numbers obtained in the tunnel began to

fall below the isentropic curve but still above the adiabatic curve to pressure tap number 9. The maximum Mach number of 2.275 was obtained at pressure tap number 7. The decrease in Mach number at taps number 10 and 24 is unexplained. This decrease in Mach number at these pressure taps appeared consistently in all runs made during the evaluation of the tunnel.

An attempt was made to maintain a constant Mach number in the test section by increasing the height of the variable area diffuser. The results of this run are shown graphically in Figure 21 and in tabular form in Table VII. Because of design limitations, the diffuser height could not exceed 1.883 inches. The calculated maximum height of the diffuser to maintain a constant Mach number in the test section including the effects of friction was 2.145 inches, Appendix F, based on a friction factor of $\overline{4f} = 0.01$. Table IV presents the diffuser coordinates vs. diffuser length in tabular form while Figure 19b presents the same data in graphical form. Examination of Figure 21 indicates a definite drop in Mach number between the nozzle exit and tap 24, in much the same manner as the drop for constant diffuser area, Figure 20, between the same pressure tap locations. As the diffuser did not increase in height appreciably in the first 1.5 inches of diffuser length, the effect of friction was to continually reduce the Mach number. Recovery of the Mach number was accomplished shortly after the diffuser height began to increase. The recovered Mach number is somewhat higher than that for constant

diffuser area, and appears to be maintaining a more constant value, thus indicating the effect of increasing the area of the diffuser. Had it been possible to increase the diffuser height to the calculated height of 2.145 inches, the resulting Mach number would have been increased much more. Until the behavior in Mach number without area change can be explained, the effect of changing the area of the diffuser can not be adequately predicted.

Figure 24 is a plot of adiabatic Mach numbers vs. distance from the tunnel nozzle throat for two operating conditions: (1) the diffuser height set at constant 1.718 inches and a back pressure of 38.98 inches of mercury, and (2) the diffuser set at the minimum starting height of 1.40 inches with a back pressure of 30.54 inches of mercury. The minimum diffuser height was based on the actual minimum height required to operate the tunnel supersonically in the test section confirmed by the calculated height in Appendix F. The calculated minimum height for isentropic flow was found to be 1.33 inches; while that for adiabatic flow was 1.40 inches, Appendix F. Table III gives the diffuser coordinates in tabular form and Figure 19b presents the same information graphically. It should be noted there was very little change of area of the diffuser near the nozzle outlet when adjustment of the diffuser height was made downstream.

The data followed the predicted curves in much the same general pattern as when the tunnel was operating under

a constant diffuser height shock free condition. The characteristic drop in Mach numbers may be noted at pressure taps 10 and 24. A predicted adiabatic Mach number at the diffuser throat was calculated with the diffuser height set at 1.40 inches, Appendix F. This predicted value of $M = 1.64$ does not correlate too well with the value of $M = 1.34$ obtained in the tunnel as shown in Figure 24.

While operating supersonically, the tunnel had a mass flow rate ranging from 0.25 lbm/sec. to 0.36 lbm/sec., as determined by the use of an orifice meter. The corresponding stagnation pressure varied from 62 to 88 inches of mercury. The mass rate of flow for the orifice meter may be determined by the procedure outlined in Appendix C, or the ideal mass rate of flow for the tunnel nozzle throat, as determined by Fliegner's formula, may be corrected by the use of the empirical Coefficient of Discharge presented graphically in Figure 25.

The average friction factor $4\bar{f}$, in the diffuser section was found to be 0.01865 when the tunnel was operating shock free supersonically, Appendix F. The diffuser height was maintained at a constant 1.718 inches and the data from Table V utilized. All predictions made involving the use of friction were based on the assumption the mean friction coefficient $4\bar{f}$ was 0.01 and was constant at this value.

Figures 22 and 23, and Table IX present the results of a pressure traverse of the tunnel operating with a

normal shock in the tunnel nozzle. Figure 22 is a plot of the Mach number vs. distance from the nozzle throat. The solid line represents the isentropic case assuming a single normal shock occurring at M = 2.05 and the dashed line the adiabatic case assuming a normal shock at M = 2.00. Immediately downstream of the single shock the isentropic Mach number will be decreased at 0.569 and continue to decrease in the nozzle, due to the increasing area, until it reaches a value of 0.388 at the end of the nozzle; the isentropic Mach number then remains constant in the diffuser section. For the adiabatic case, the Mach number immediately downstream of the shock will be 0.577, based on the shock occurring at M = 2.00. The Mach number continues to decrease for the subsonic flow but at a slower rate. Between pressure taps 9 and 15, the area change is slight and the Mach number remains constant at M = 0.429. In the constant area diffuser, the adiabatic Mach number is increased due to the frictional effects. As shown in the Schlieren photographs by the repeated shock pattern, Figures 13 to 18, the flow conditions through a normal shock are definitely not a simple one dimensional process. A shock occurs and the flow immediately goes subsonic. Due to inner action with the boundary layer, the flow accelerates to a lower supersonic value and the process is repeated until the flow remains subsonic. The overall effect of Mach number reduction caused by the multiple shocks is shown in Figure 22. Due to the complex inner action of the normal shocks and the

oblique shocks with the boundary layer, and the change of stagnation pressure for each shock occurring, definite determination of the Mach number through a shocking system is difficult. The method for calculating the Mach numbers of Figure 22 is presented in Appendix F.

At a Mach number exceeding 1.00 the effect of friction is to reduce the Mach number to a limiting value of 1.00. At Mach numbers lower than unity, the effect of friction is reversed; namely, the subsonic flow is accelerated to a limiting Mach number of 1.00. This increase of Mach number due to the effects of friction on subsonic flow may be noted by the gradual increase of Mach number of the subsonic flow in Figure 22 or in Table IX.

Figure 23 is a plot of the tunnel pressure ratios based on the stilling tank stagnation pressure vs. distance from the nozzle throat for the cases of shock free and shock in the nozzle operations. The pressure ratio pattern for shock free operation follows the isentropic curve closely with deviations commencing about four inches from the nozzle throat. With shock in the nozzle operation, failure of the pressure ratio downstream of the shock to recover to the isentropic value is a loss of stagnation pressure caused by the repeated shock pattern.

Conclusions and Recommendations

A. Conclusions.

1. The qualitative and quantitative evaluation of the tunnel system as installed, show it to be a suitable laboratory device for the study of compressible fluid flow.

2. The minimum starting height of the variable area diffuser was found to be 1.40 inches.

3. The average friction factor, $4\bar{f}$, was found to be 0.02044, but is believed high in value.

4. Schlieren photographs of the flow field may be taken in black and white or in color.

5. A vertical knife edge orientation in the Schlieren system is best for studying shock phenomenon.

6. A horizontal knife edge orientation in the Schlieren system is best for studying the boundary layer.

7. The sharpness of the Schlieren photographs is poor due to the use of non-collimated light and the light beam passing through the tunnel test section twice.

8. The phenomenon of a standing shock is definitely not one dimensional.

B. Recommendations.

It is recommended the following modifications for improving the performance and usefulness of the tunnel system be undertaken:

1. An additional relay be installed on the Bailey stagnation pressure controller to maintain a more uniform stagnation pressure.

2. Additional heat capacitors be installed in the receivers to maintain a more constant stagnation temperature.

3. A total pressure probe be installed in the fixed geometry diffuser to obtain the back pressure stagnation pressure.

4. For more quantitative visual results, the Schlieren system be modified to a single pass parallel light beam system.

5. A more rapid means of obtaining the differential pressure measurements be installed.

6. The camera system be modified to a reflex type system.

7. An additional oil filter be installed.

8. Additional pressure taps be installed downstream of the variable area diffuser in the existing pressure survey tunnel sidewall.

9. The geometry of the variable area diffuser be modified to permit constant Mach number runs.

BIBLIOGRAPHY

1. Alan Pope, "Wind-Tunnel Testing", John Wiley & Sons, Inc., 1950.

2. A. H. Shapiro, "The Dynamics and Thermodynamics of Compressible Fluid Flow", Volume I, Ronald Press Co., 1953.

3. J. H. Keenan and J. Kaye, "Gas Tables", John Wiley & Sons, Inc., 1957.

4. The American Society of Mechanical Engineers, "Fluid Meters, Their Theory and Application", American Society of Mechanical Engineers, 1959.

5. The American Society of Mechanical Engineers, "Instruments and Apparatus--Chapter Four Fluid Measurement, Supplement to ASME Power Test Codes," The American Society of Mechanical Engineers, 1959.

6. J. J. Smolderen, AGARDograph 17, Condensation Effects and Air Drying Systems for Supersonic Wind-Tunnels, North Atlantic Treaty Organization Advisory Group for Aeronautical Research and Development, 1956.

7. D. W. Holder, R. J. North and G. P. Wood, AGARDograph 23, Optical Methods for Examining the Flow in High-Speed Wind Tunnels, North Atlantic Treaty Organization Advisory Group for Aeronautical Research and Development, 1956.

8. Lee Arnold, AGARDograph 11, Dynamic Measurements in Wind Tunnels, North Atlantic Treaty Organization Advisory Group for Aeronautical Research and Development, 1955.

9. J. A. Hill, J. R. Baron, L. H. Markham, AGARDograph 22, Mach Number Measurements in High Speed Wind Tunnels, North Atlantic Treaty Organization Advisory Group for Aeronautical Research and Development, 1956.

10. A. Ferri and S. M. Bogdoroff, AGARDograph 1, Design and Operation of Intermittent Supersonic Wind Tunnels, North Atlantic Treaty Organization Advisory Group for Aeronautical Research and Development, 1954.

11. J. Lukasiewicz, Development of Large Intermittent Wind Tunnels, Journal of the Royal Aeronautical Society, Number 532, Volume 59, pp. 259-278, April 1955.

12. T. W. Macios, Supersonic-Wind-Tunnel-Air-Drying-System Design, ASME Paper No. 59-A-161, The American Society of Mechanical Engineers, 1959.

13. Ames Aeronautical Laboratory Drawings AD-10234-D1 and D2, Ames Aeronautical Laboratory, 1952.

14. C. C. Perry and H. R. Lissner, The Strain Gage Primer, McGraw Hill Book Co., 1955.

15. Charles J. Muto, An Experimental Investigation of the Effects of Heat Transfer During Charging and Blowdown of Single Gas Receivers, M. S. Thesis, U. S. Naval Postgraduate School, Monterey, California, 1959.

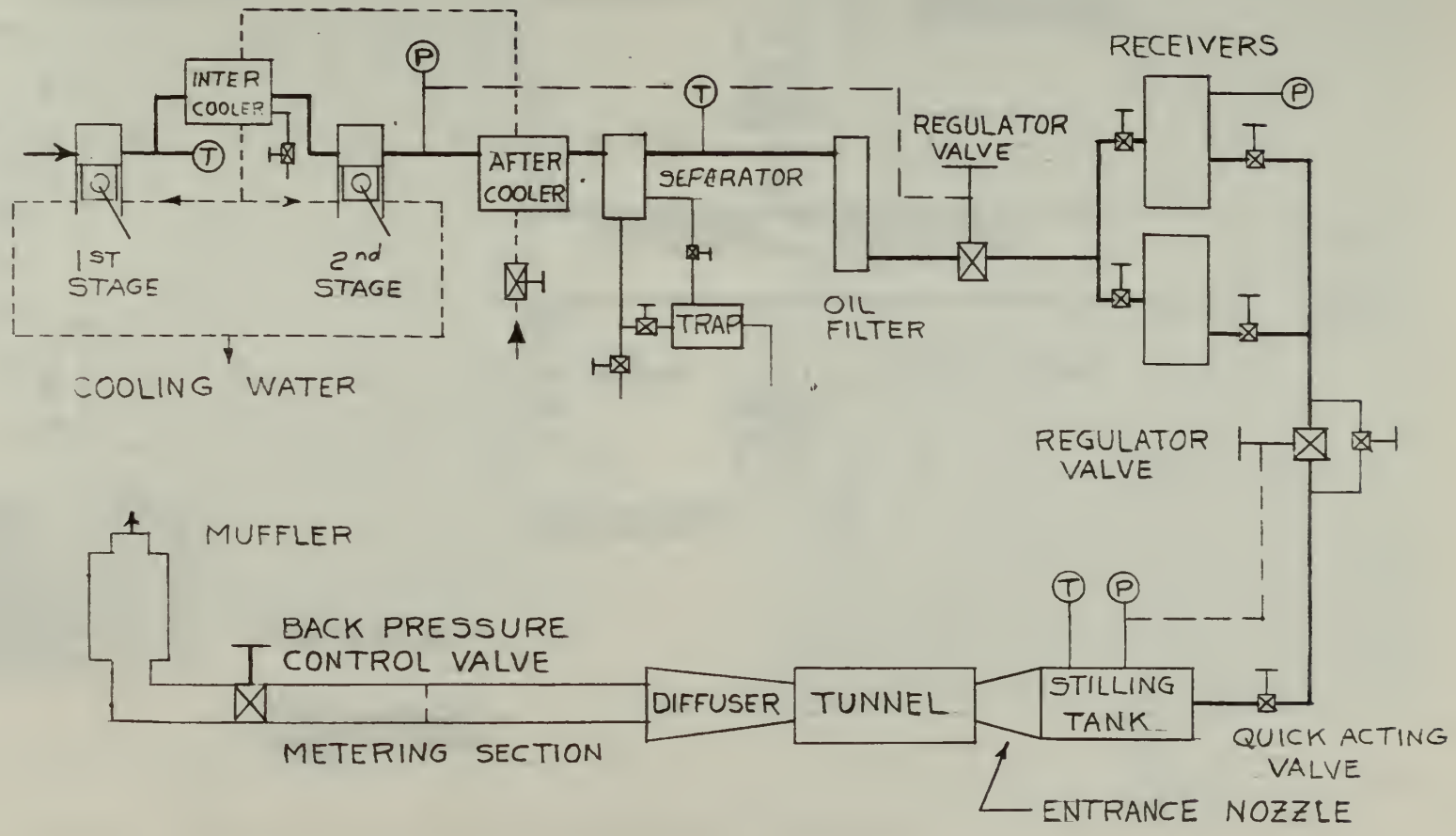

Figure 1. Schematic Diagram of the Tunnel System

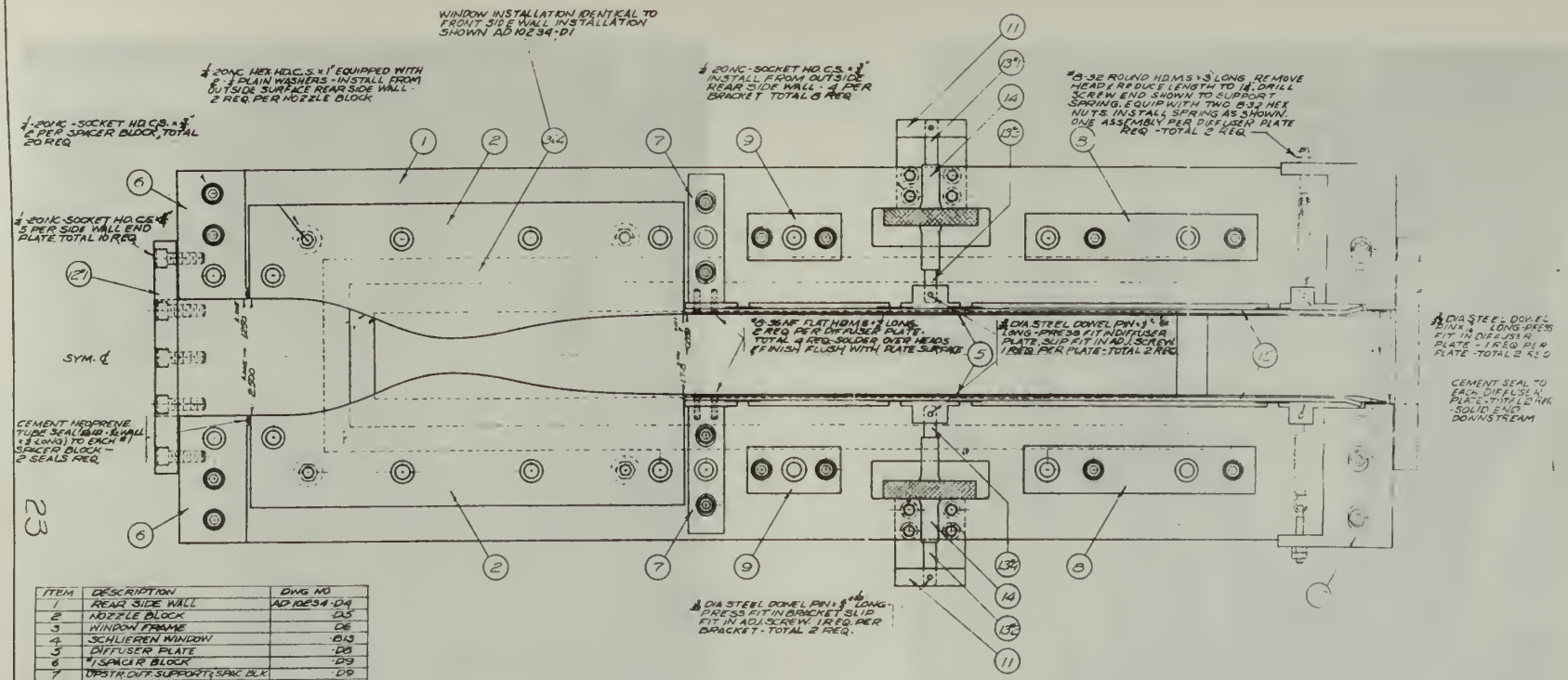

ITEM	DESCRIPTION	DWG NO
1	REAR SIDE WALL	AD 10234-D4
2	NOZZLE BLOCK	-D5
3	WINDOW FRAME	-D6
4	SCHLIEREN WINDOW	-B13
5	DIFFUSER PLATE	-D8
6	#1 SPACER BLOCK	-D9
7	UPSTR. DIFF. SUPPORT & SPAC BLK.	-D9
8	#3 SPACER BLOCK	-D9
9	#2 SPACER BLOCK	-D9
10	DOWNSTR. DIFF. SUPPORT & SPAC. BLK.	-D10
11	DIFFUSER ADJUST. BRACKET	-D10
12	SIDE WALL END PLATE	-D10
13	DIFFUSER ADJUST. SCREW	-D10
14	DIFFUSER PLATE ADJUSTMENT	-D11
15	DIFFUSER PLATE SEAL	-B12

GASKET NOTE

CEMENT 0.015 VELLUMOID TO BOTH SIDES OF ITEMS 2, 6, 7 & 10, ALLOWING FOR BOLT & SCREW HOLES

PIN NOTE

TEST RUNS WILL DETERMINE OPTIMUM POSITIONS OF ALL PARTS. PARTS (ITEMS 2, 6, 7 & 10) SHALL BE PINNED IN THESE POSITIONS WITH #10 TAPER PINS 1" LONG, 2 PINS PER PART, TOTAL 16 PINS REQ

Figure 2. Test Section Subassembly

AMES AEROSPACE - CA.

AD-

SHEET OF

AD- 10234-D2

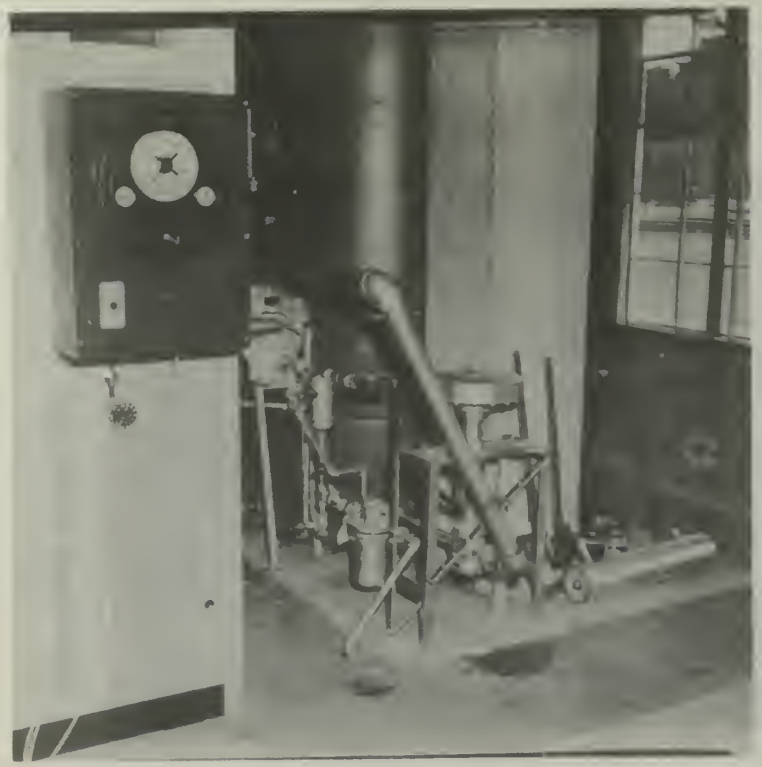

Figure 3. Compressor Discharge Pressure Control and Air Drying System.

Figure 4. Tunnel Section Stagnation' Pressure Control System.

Figure 5. Stilling Tank.

Figure 10. Manometer Manifolds

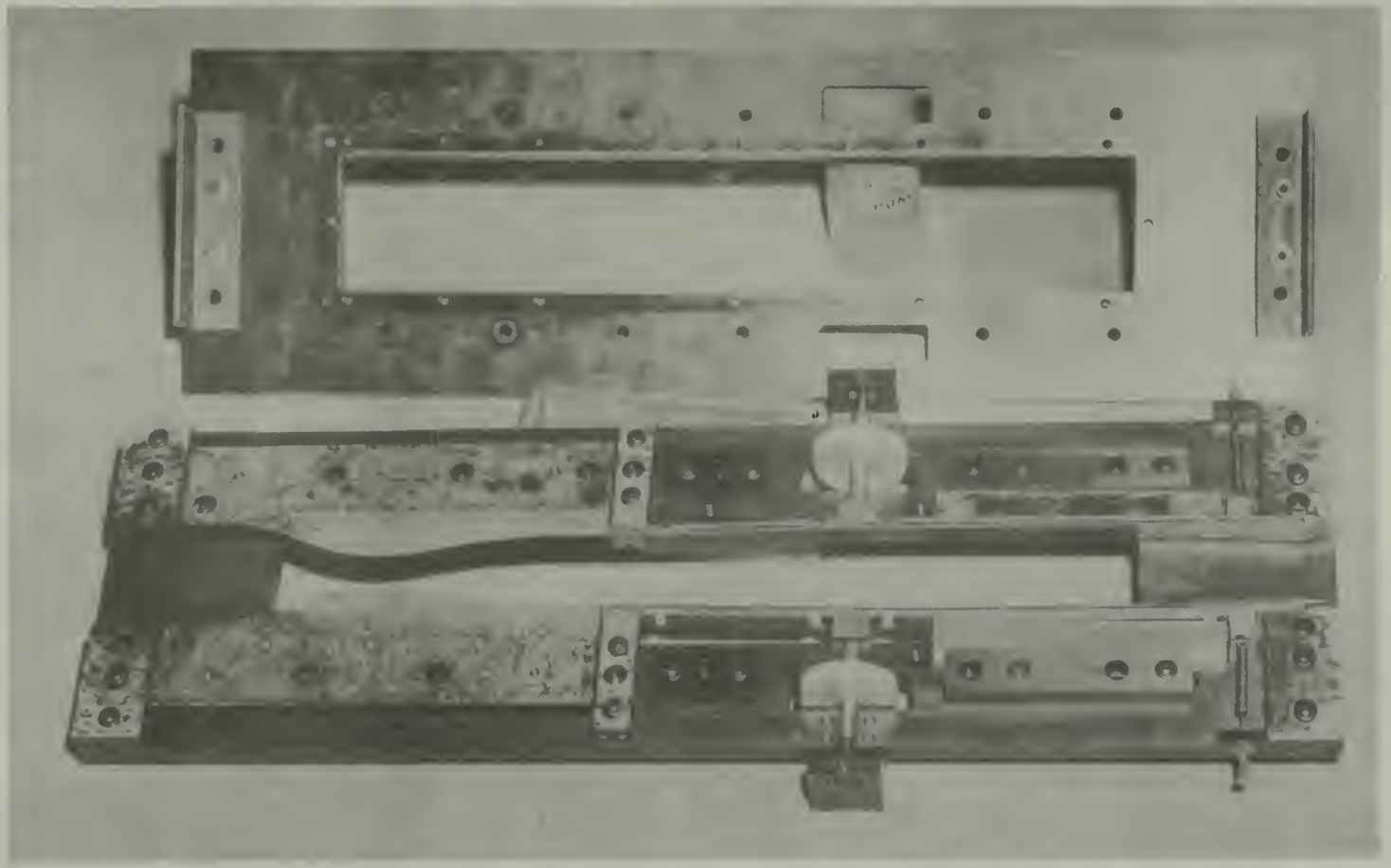

Figure 6. Test Section, Disassembled

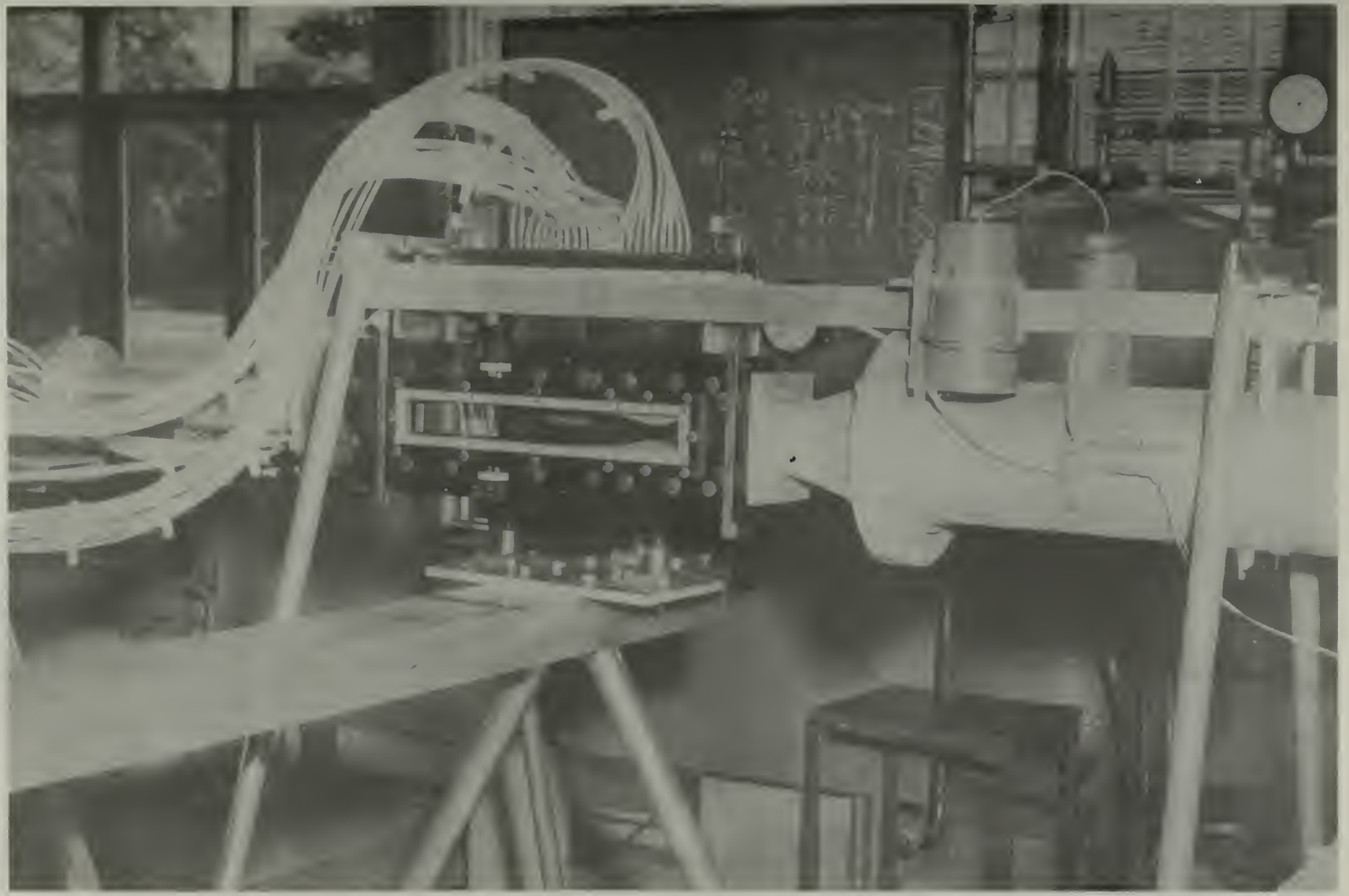

Figure 7. Stilling Tank, Entrance Nozzle, Test Section, and Diffuser Assembly.

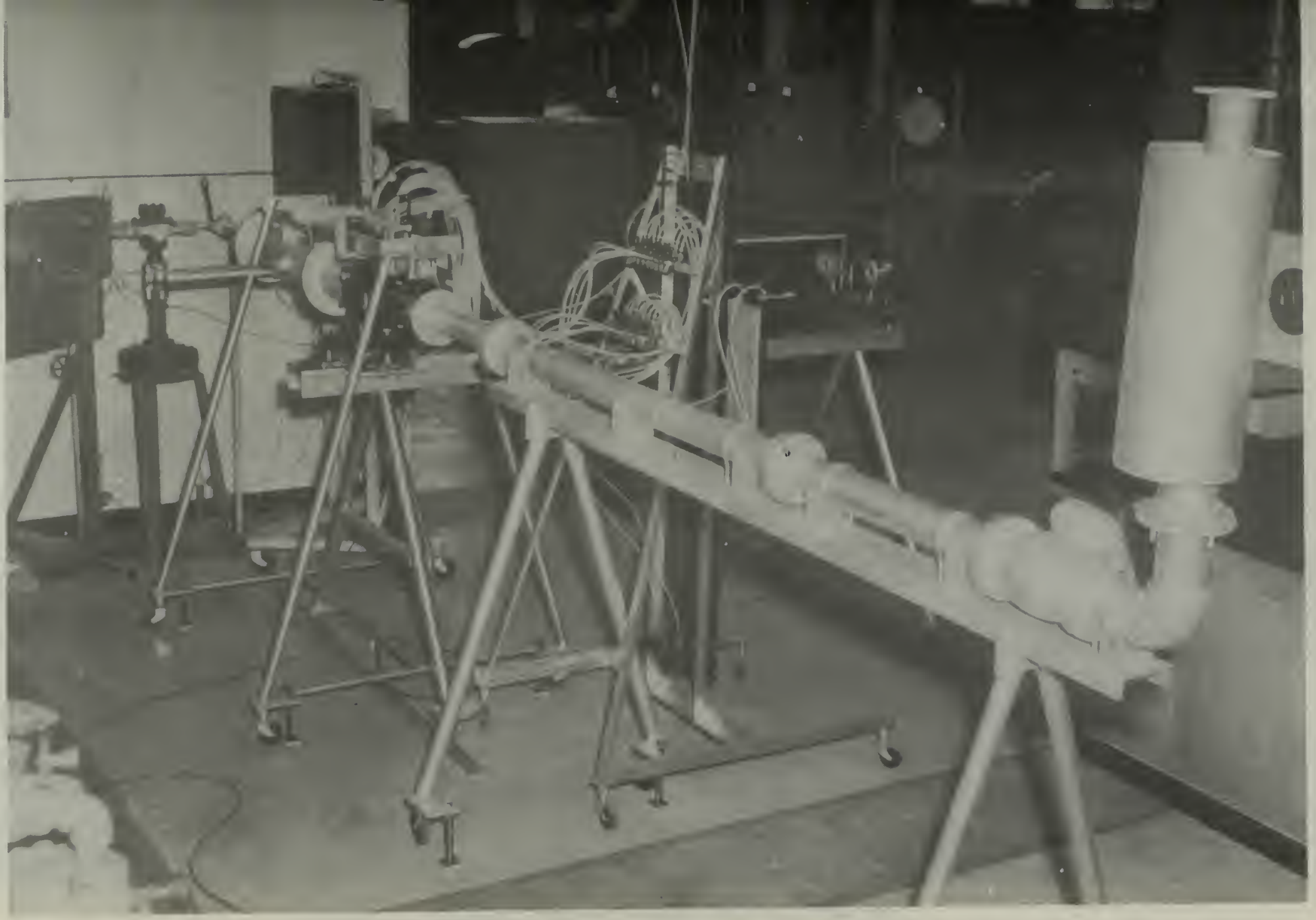

Figure 9. Overall View of Tunnel Section from Front Side.

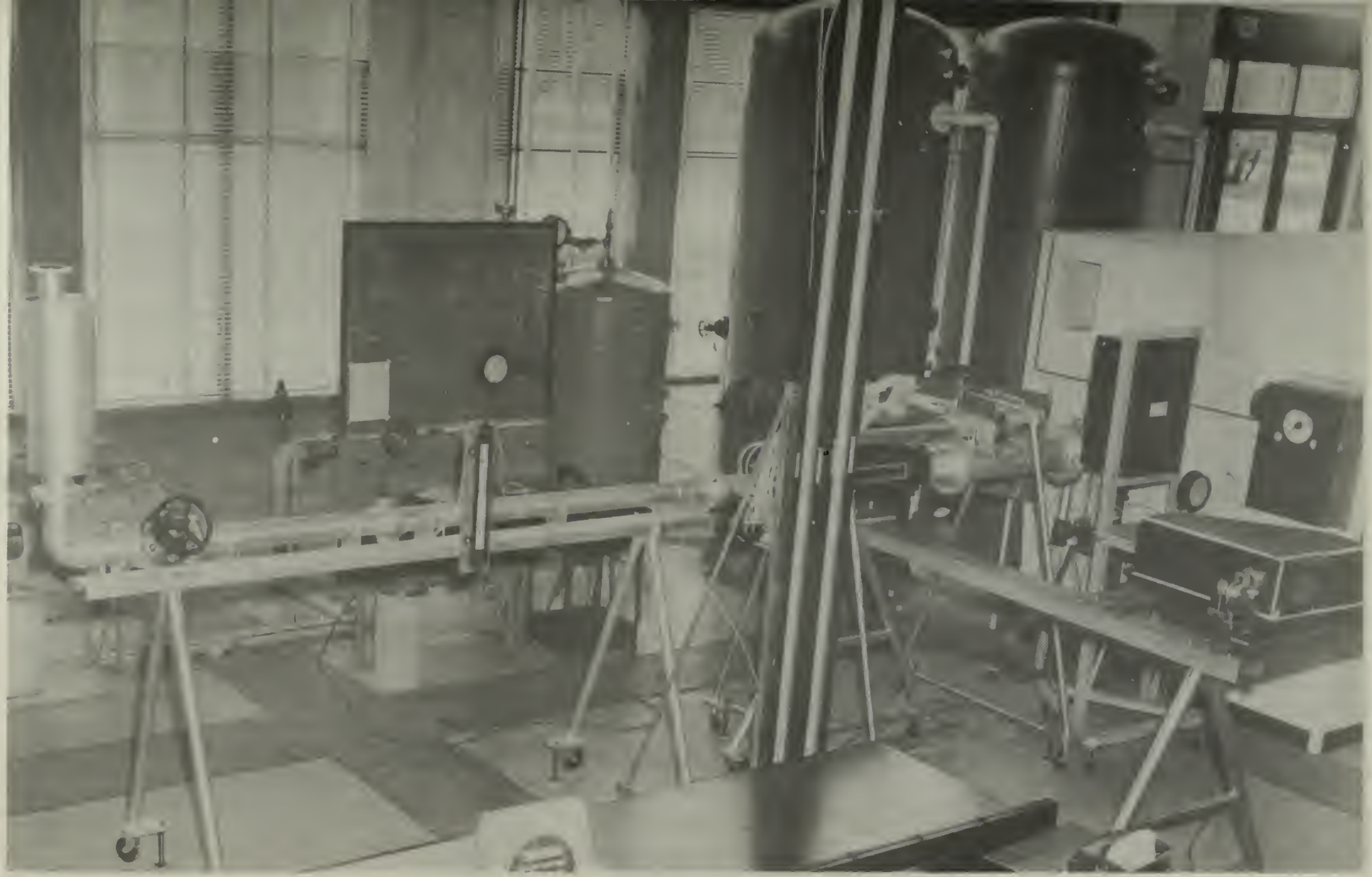

Figure 8. Overall View of Tunnel Section from Rear Side.

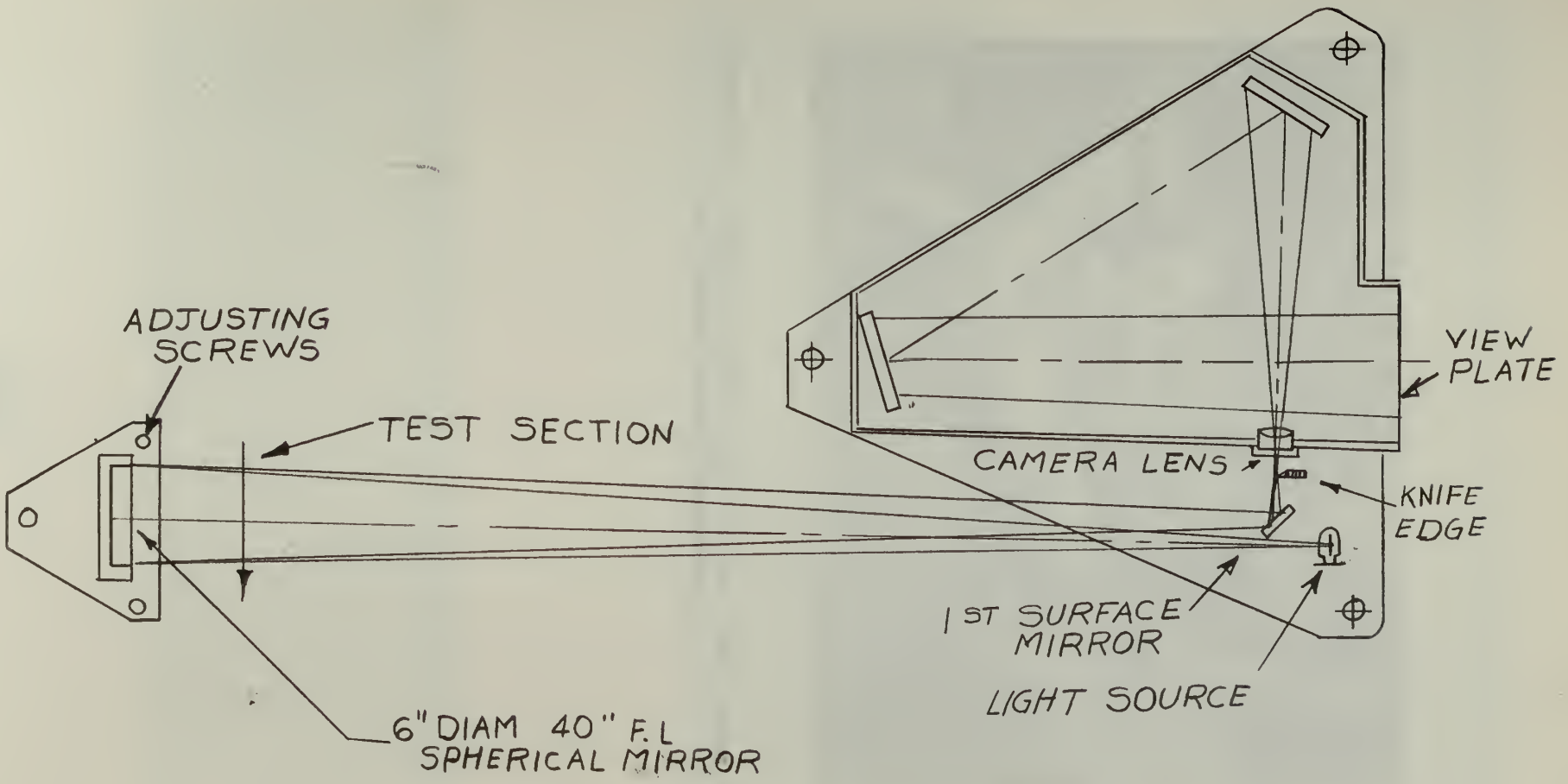

FIG. 11. SCHLIEREN CAMERA SYSTEM

Figure 12. Schlieren System Light Source, Knife Edge, and Camera-Viewing Components.

A. Vertical Knife. P_o = 71.46 in Hg. a., P_b = 30.92 in. Hg. a., T_o = 61.1° F. Nozzle Running Shock Free with Air Flow Right to Left. Note Strong Mach Wavelet Originating at Junction of Nozzle and Test Section. See Figure 18.

B. Vertical Knife. P_o = 72.31 in Hg. a., P_b = 30.92 in. Hg. a., T_o = 59.23° F. Tunnel Running Shock Free With Air Flow Right to Left.

C. Horizontal Knife. P_o = 72.71 in. Hg. a., P_b = 30.92 in. Hg. a., T_o = 65.5° F. Tunnel Running Shock Free With Air Flow Right to Left. Note Thickness of the Boundary Layers.

Figure 13. Tunnel Running Shock Free

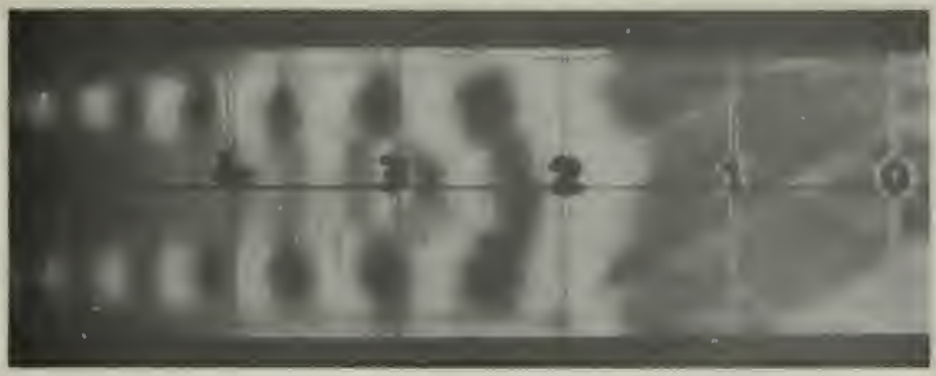

A. Vertical Knife. P_o = 67.35 in. Hg. a., P_b = 30.45 in. Hg. a., T_o = 66.3° F.
Diffuser Height 1.718 inches. Normal Shock at Station 12.

B. Horizontal Knife. P_o = 67.41 in. Hg. a., P_b = 30.86 in. Hg. a., T_o = 65.9° F.
Diffuser Height 1.718 inches. Normal Shock at Station 12.

C. Vertical Knife. P_o = 81.52 in. Hg. a., P_b = 38.32 in. Hg. a., T_o = 57.0° F.
Diffuser Height 1.718 inches. Due to Higher Density and Reynolds Number Shock has Moved Upstream as Compared to Figure 14A.

Figure 14. Effect of Increased Back Pressure on Shock Location

A. Vertical Knife. P_o = 65.35 in. Hg. a., P_b = 30.65 in. Hg. a., T_n = 59.6° F. Boundery Layer Vieible on Nnzzle Walls and Incraesing in Thicknese Downstraem of Shnck.

B. Horizontel Knife. P_o = 64.41 in. Hg. a., P_b = 30.83 in. Hg. a., T_o = 63.2° F. Note Pull off of Boundery Layer at Shock and Asymmetrical Shading of Corras-pnnding Parts on Oppnsite Sidas of Tunnal Centerline. Shock is Moving Tnwards Nozzle Throat as P_o is Decreasad from Figure 15 A.

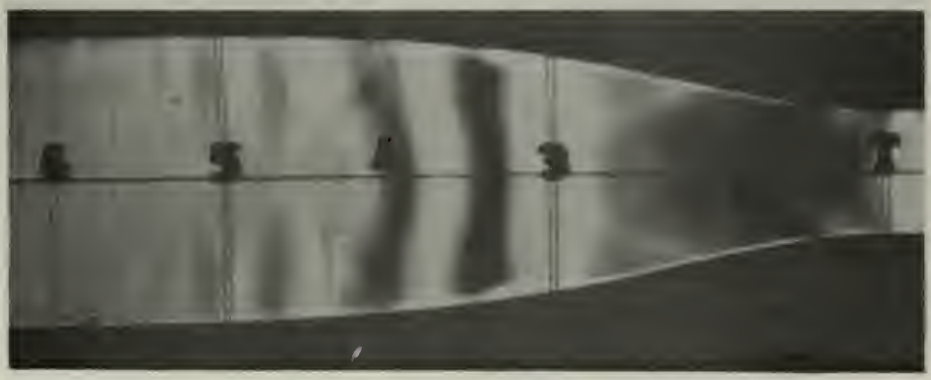

C. Vertical Knife. P_o = 59.96 io. Hg. a., P_b - 30.73 in. Hg. a., T_n = 61.8° F. Weakar Shock Moving Upstreem as P_n is Reduced an Additional Amount.

Figura 15. Effect nf Reducing Stagnatioo Pressure for Shnck io Nnzzle

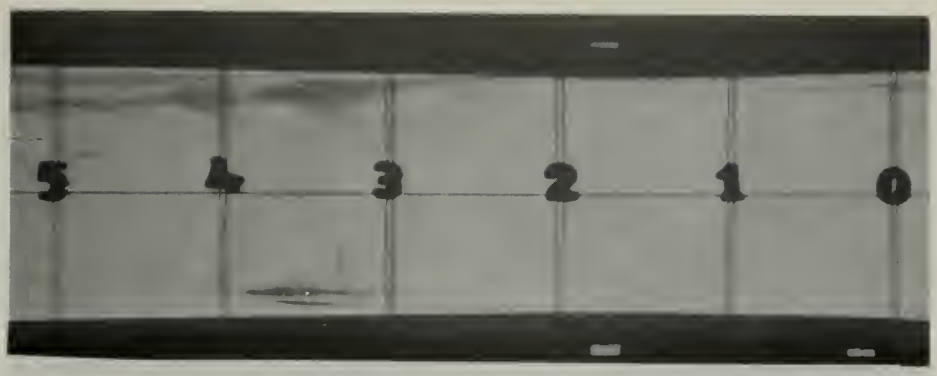

A. Vertical Knife. P_o = 82.71 in. Hg.a., T_o = 57.6° F, Diffuser Height = 1.39 in. Shock Could not be Blown Through Diffuser Nozzle.

B. Vertical Knife. P_o = 60.26 in. Hg. a., T_o = 58.6° F. Diffuser Height = 1.40 in. Area has been Increased 0.005 Square Inches Compared to Figure 16 A, and Shock has been Blown Through Diffuser Nozzle. Pressure Could be Reduced more to move Shock towards the Throat.

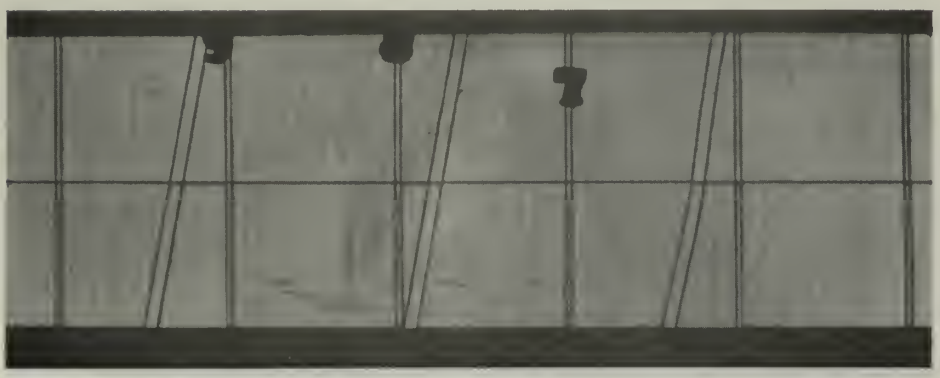

C. Tunnel not Running. Knife Edge not Inserted. Effect of Non-Parallel Two Pass Light is Evident. Double Vertical Lines are Images of Wires Placed on Spherical Mirror Side of Schlieren Window. Diagonal Lines are Images of Wires Placed on Light Source Side of Schlieren Window. Light Passing These Wires had to Travel Farther before Striking Spherical Mirror and Hence More Deflection of the Image.

Figure 16. Effect of Area Change on Shock Location in Diffuser Nozzle.

A. Vertical Knife. P_o = 60.00 in. Hg. a., T_o = 55.0° F. Diffuser Height = 1.42 inches. Shock Pulled Back Through Diffuser Nozzle when P_o was Decreased to 59.50 in. Hg. a.

B. Horizontal Knife. P_o = 60.61 in. Hg. a., T_o = 63.1° F. Diffuser Height = 1.47 inches. Note Strong Pull Off of Boundary Layer at Station 12.25.

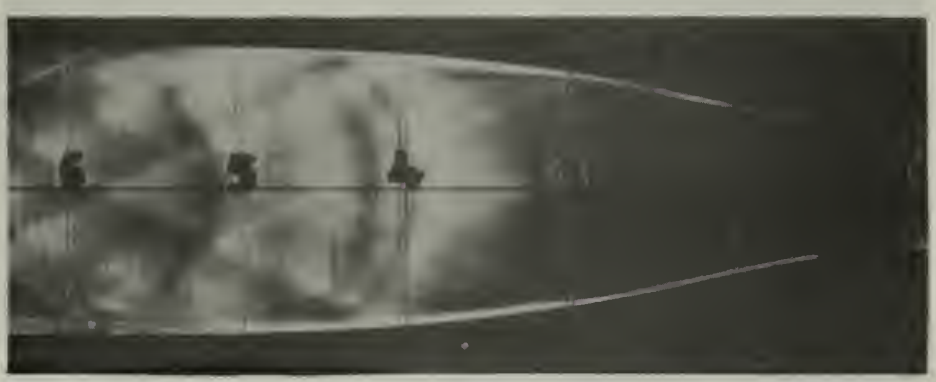

C. Vertical Knife. P_o = 72.31 in. Hg. a., T_o = 58.7° F. Dark Concave Lines at Stations 4 and 5 are the Result of Oil Film Deposit on Walls. Dark Horizontal Lines Starting at Station 3 are also oil Streaks on Schlieren Walls.

Figure 17. Tunnel Running With Reduced Diffuser Area.

A. Vertical Knife. P_o = 71.46 in. Hg. a. P_b = 30.92 in. Hg. a. T = 61.1° F. Air Flow is Right to Left. Section is an Enlargement of Figure 13 A. Nozzle is Running Shock Free. Mach Number determined from Wavelets by Relationship $\sin \alpha = \frac{1}{M}$. At Corresponding Point Adiabatic Mach Number is 2.125.

B. Vertical Knife. P_o = 72.31 in. Hg. a., P_b = 30.92 in. Hg. a., T_o = 59.23° F. Air Flow is Right to Left. Section is an Enlargement of Figure 13B. At Corresponding Point Adiabatic Mach Number is 1.828.

Figure 18. Determination of Mach Number from Mach Wavelets.

A. Vertical Knife. P_o = 71.46 in. Hg. a. P_b = 30.92 in. Hg. a. T = 61.1° F. Air Flow is Right to Left. Section is an Enlargement of Figure 13 A. Nozzle is Running Shock Free. Mach Number determined from Wavelets by Relationship $\sin \alpha = \frac{1}{M}$. At Corresponding Point Adiabatic Mach Number is 2.125.

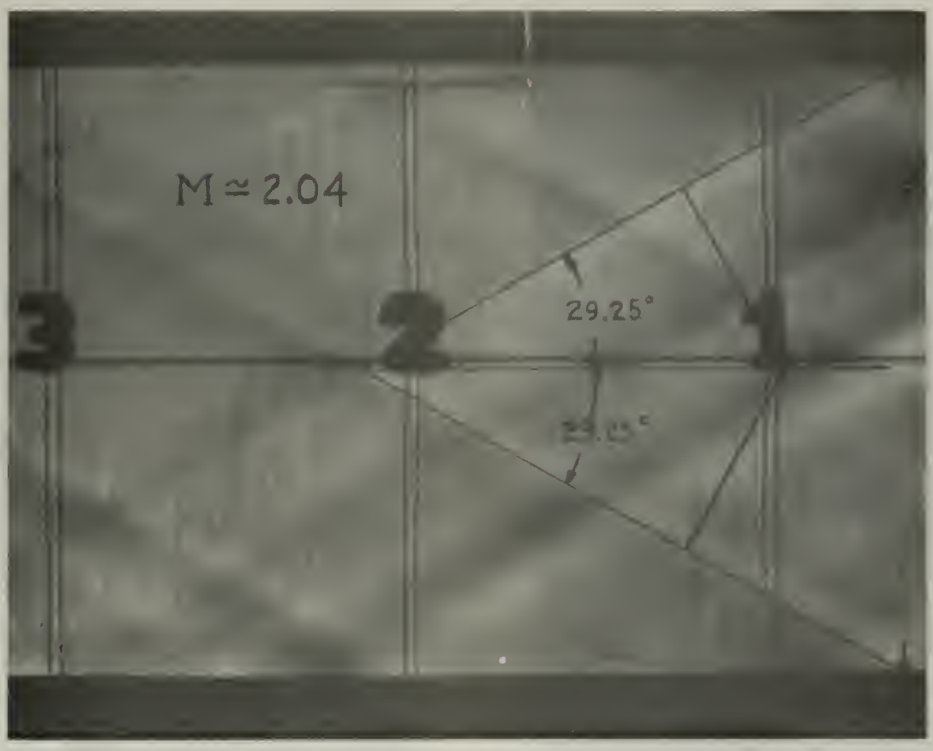

B. Vertical Knife. P_o = 72.31 in. Hg. a., P_b = 30.92 in. Hg. a., T_o = 59.23° F. Air Flow is Right to Left. Section is an Enlargement of Figure 13B. At Corresponding Point Adiabatic Mach Number is 1.828.

Figure 18. Determination of Mach Number from Mach Wavelets.

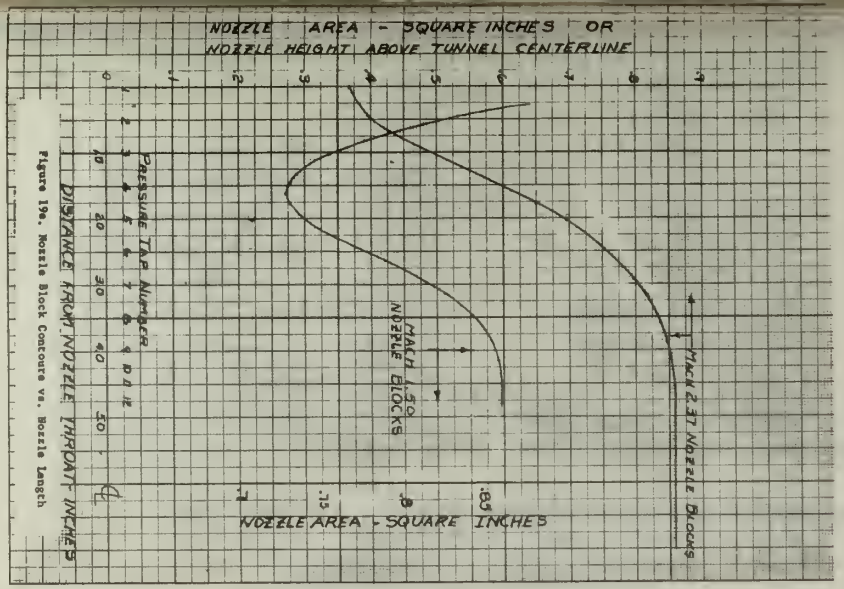

Figure 19a. Nozzle Block Contours vs. Nozzle Length

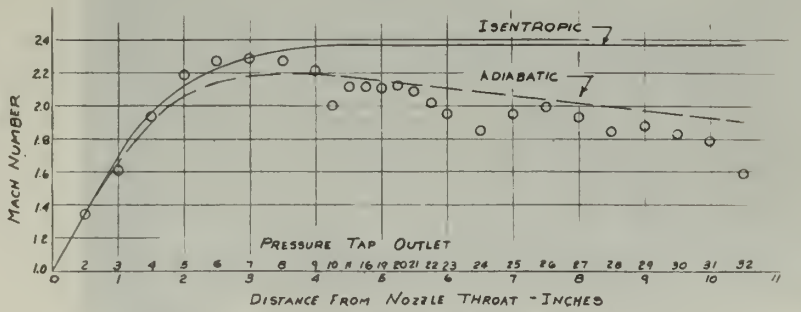

Figure 20. Adiabatic Mach Number vs. Tunnel Length Compared to Theoretical Mach Number Using 2.37 Nozzle Blocks and Diffuser Height = 1.718 Inches.

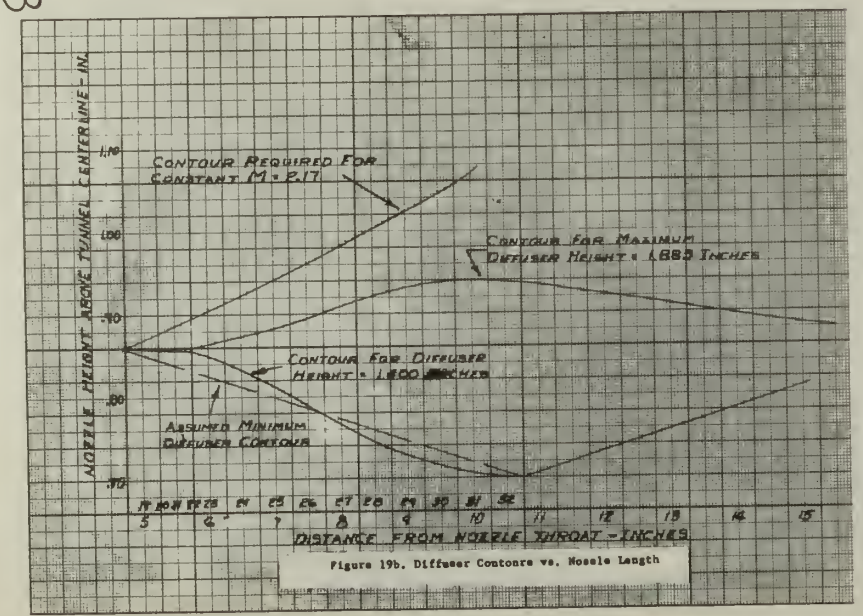

Figure 19b. Diffuser Contours vs. Nozzle Length

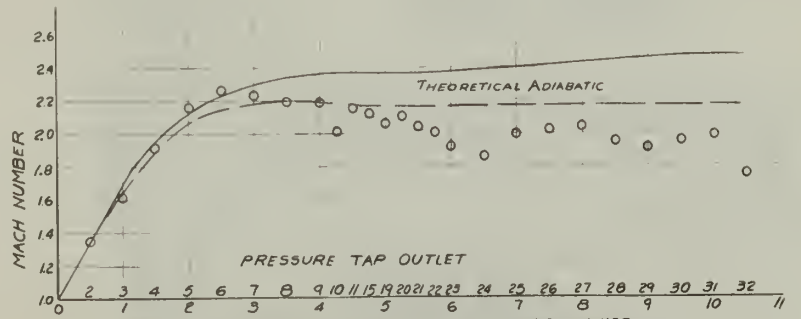

Figure 21. Adiabatic Mach Number vs. Tunnel Length Compared to Theoretical Mach Number Using 2.37 Nozzle Blocks and Diffuser Height = 1.883 Inches.

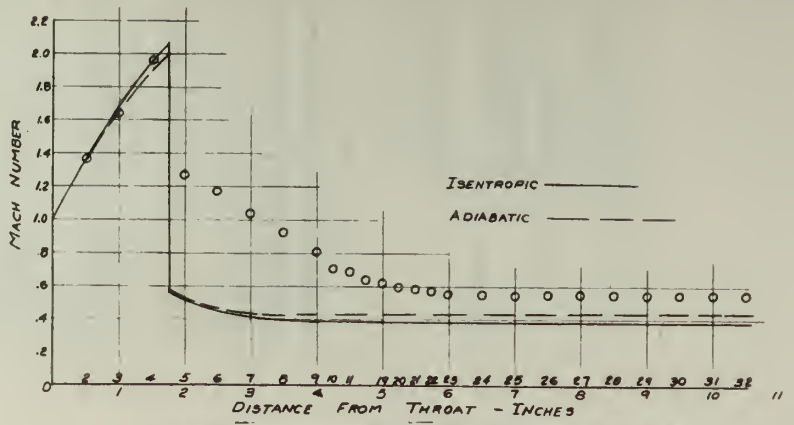

Figure 22. Adiabatic Mach Number vs. Tunnel Length Compared to Theoretical Mach Number With a Normal Shock Standing in Nozzle.

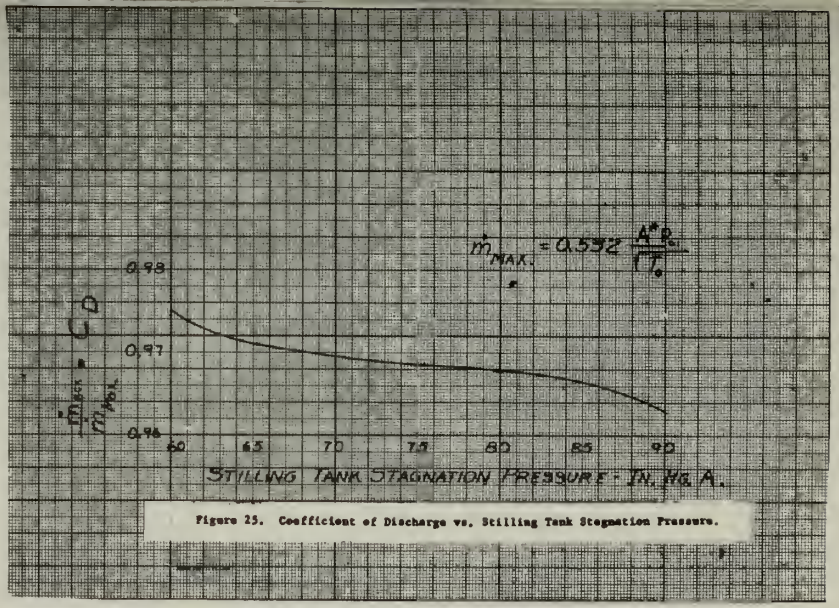

Figure 25. Coefficient of Discharge vs. Stilling Tank Stagnation Pressure.

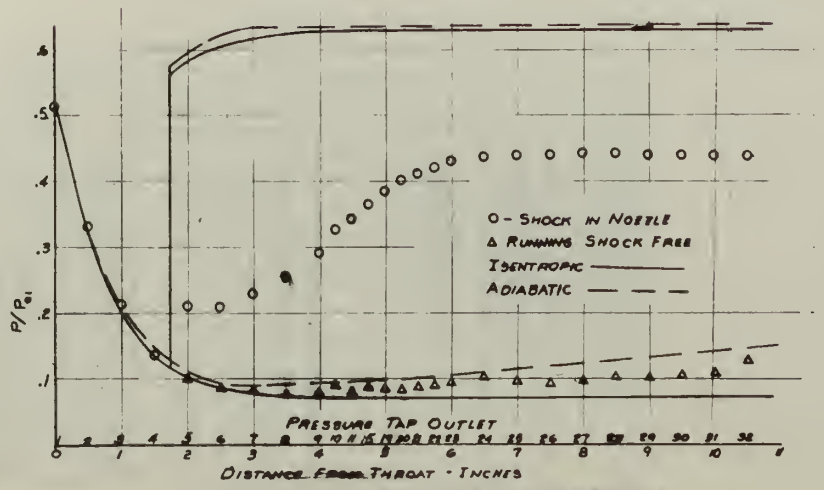

Figure 23. Tunnel Pressure Ratios vs. Tunnel Length With and Without A Normal Shock in Nozzle Using 2.37 Nozzle Blocks.

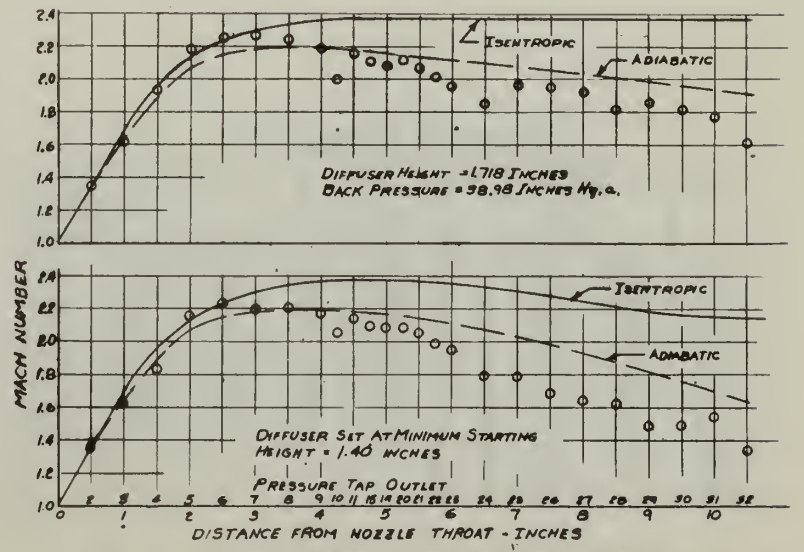

Figure 24. Adiabatic Mach Number vs. Tunnel Length Compared to Theoretical Mach Number Using 2.37 Nozzle Blocks, Varying Back Pressure, and Setting Diffuser Height = 1.40 Inches.

TABLE I
Design Data for Mach 2.37 Nozzle Blocks

Distance from Throat, in	A in.^{2}	A/A*	M Isen-tropic	P/P$_{ol}$ Isen-tropic	Tap No.	Distance from Throat, in.	A in.^{2}	A/A*
0.000	0.367	1.000	1.000	0.5283	1	0.000	0.367	1.000
0.225	0.374	1.019	1.157	0.4359	2	0.500	0.402	1.097
0.450	0.394	1.073	1.315	0.3536	3	1.000	0.492	1.340
0.675	0.427	1.162	1.478	0.2812	4	1.500	0.595	1.621
0.900	0.470	1.280	1.636	0.2230	5	2.000	0.691	1.883
1.126	0.519	1.415	1.778	0.1800	6	2.500	0.756	2.060
1.351	0.568	1.548	1.894	0.1506	7	3.000	0.804	2.190
1.596	0.614	1.670	1.987	0.1304	8	3.500	0.834	2.271
1.801	0.656	1.788	2.069	0.1148	9	4.000	0.850	2.315
2.026	0.694	1.890	2.133	0.1039	10	4.250	0.855	2.330
2.251	0.726	1.978	2.185	0.0957	11	4.500	0.857	2.335
2.476	0.754	2.050	2.225	0.0899	12-18	4.750	0.859	2.340
2.701	0.778	2.120	2.264	0.0846				
2.926	0.798	2.175	2.291	0.0811				
3.151	0.815	2.220	2.315	0.0781				
3.376	0.828	2.255	2.331	0.0762				
3.602	0.839	2.285	2.345	0.0745				
3.827	0.847	2.305	2.354	0.0735				
4.052	0.853	2.320	2.364	0.0724				
4.277	0.856	2.330	2.367	0.0720				
4.539	0.858	2.337	2.369	0.0718				
4.802	0.859	2.340	2.371	0.0716				

TABLE II
Design Data for Mach 1.50 Nozzle Blocks

Distance from throat, in.	A in.^{2}	A/A*	M Isen-tropic	P/P$_{ol}$ Isen-tropic	Tap No.	Distance from throat, in.	A in.^{2}	A/A*
0.000	0.729	1.000	1.000	0.5283	1	-1.601	0.931	1.279
0.171	0.731	1.003	1.019	0.5166	2	-1.101	0.833	1.142
0.343	0.736	1.012	1.125	0.4540	3	-0.601	0.758	1.041
0.604	0.748	1.025	1.181	0.4277	4	-0.101	0.730	1.001
0.686	0.760	1.042	1.237	0.3928	5	0.399	0.740	1.015
0.857	0.774	1.061	1.287	0.3673	6	0.899	0.776	1.065
1.029	0.789	1.081	1.333	0.3450	7	1.399	0.816	1.120
1.200	0.802	1.100	1.372	0.3268	8	1.899	0.843	1.154
1.372	0.814	1.115	1.400	0.3142	9	2.399	0.656	1.174
1.543	0.825	1.132	1.430	0.3012	10	2.649	0.858	1.176
1.715	0.834	1.143	1.449	0.2931	11	2.899	0.859	1.178
1.886	0.842	1.155	1.468	0.2853	12-18	3.149	0.859	1.178
2.058	0.848	1.162	1.479	0.2808				
2.229	0.852	1.169	1.466	0.2780				
2.401	0.855	1.173	1.495	0.2744				
2.562	0.857	1.175	1.498	0.2732				
2.743	0.858	1.176	1.500	0.2724				
2.915	0.859	1.178	1.503	0.2712				
3.086	0.859	1.178	1.503	0.2712				
3.201	0.859	1.178	1.503	0.2712				

TABLE III
Data for Diffuser Set at Minimum Starting Height of 1.40 inches with Mach 2.37 Nozzle Blocks

Distance from Nozzle exit in.	A in.^{2}	A/A*	M Isen-tropic	P/P$_{ol}$ Isen-tropic	Tap No.	Distance from Nozzle exit in.	A in.^{2}	A/A*
0.00	0.859	2.340	2.371	0.0716	12-18	-0.042	0.859	2.340
1.00	0.856	2.332	2.369	0.0718	19	0.208	0.858	2.337
2.00	0.821	2.240	2.323	0.0771	20	0.458	0.857	2.335
3.00	0.777	2.115	2.260	0.0851	21	0.708	0.856	2.332
4.00	0.735	2.005	2.200	0.0935	22	0.958	0.856	2.332
5.00	0.709	1.932	2.158	0.0999	23	1.208	0.847	2.308
6.00	0.700	1.908	2.144	0.1021	24	1.708	0.830	2.262
7.00	0.726	1.979	2.186	0.0956	25	2.208	0.813	2.215
8.00	0.751	2.050	2.225	0.0899	26	2.708	0.795	2.165
9.00	0.777	2.115	2.260	0.0850	27	3.208	0.777	2.115
10.00	0.803	2.190	2.298	0.0820	28	3.708	0.748	2.090
11.00	0.828	2.255	2.331	0.0762	29	4.208	0.727	1.980
					30	4.708	0.714	1.943
					31	5.208	0.705	1.920
					32	5.708	0.700	1.908

TABLE IV
Data for Diffuser Set at Maximum Height of 1.883 inches with Mach 2.37 Nozzle Blocks

Distance from nozzle exit, in.	A in.^{2}	A/A*	M Isen-tropic	P/P$_{ol}$ Isen-tropic	Tap No.	Distance from nozzle exit, in.	A	A/A*
0.00	0.859	2.340	2.371	0.0716	12-18	-0.042	0.859	2.340
1.00	0.858	2.339	2.371	0.0716	19	0.208	0.859	2.340
2.00	0.878	2.393	2.395	0.0689	20	0.458	0.859	2.340
3.00	0.902	2.460	2.425	0.0658	21	0.708	0.858	2.337
4.00	0.926	2.525	2.454	0.0629	22	0.958	0.858	2.337
5.00	0.941	2.565	2.470	0.0613	23	1.208	0.861	2.342
6.00	0.936	2.555	2.466	0.0617	24	1.708	0.871	2.378
7.00	0.926	2.525	2.465	0.0618	25	2.208	0.884	2.408
8.00	0.914	2.490	2.438	0.0645	26	2.708	0.896	2.441
9.00	0.900	2.455	2.423	0.0660	27	3.208	0.908	2.475
10.00	0.889	2.420	2.408	0.0676	28	3.708	0.920	2.510
11.00	0.880	2.400	2.399	0.0685	29	4.208	0.932	2.540
					30	4.708	0.940	2.560
					31	5.208	0.941	2.565
					32	5.708	0.938	2.555

TABLE V

Data Sheet for Shock Free Operation with Mach 2.37 Nozzle Blocks, Constant Diffuser Area and Minimum Back Pressure

Time Sec	T_{o1} ^{o}R	P_{o1} in. Hg.a.	Tap No.	ΔP in. Hg.	P/P_{o1}	A/A*	$\left(\frac{P}{P_{o1}}\right)\left(\frac{A}{A^*}\right)$	M	Tap No.	ΔP in. Hg.	P/P_{o1}	A/A*	$\left(\frac{P}{P_{o1}}\right)\left(\frac{A}{A^*}\right)$	M
0	526	73.78	2	49.0	0.3360	1.097	0.3685	1.346	17	67.4	0.0864	2.340	0.2020	2.091
39	525	73.78	3	57.7	0.2180	1.340	0.2920	1.608	18	68.1	0.0769	2.340	0.1800	2.261
75	525	73.68	4	63.4	0.1392	1.621	0.2259	1.936	19	67.4	0.0852	2.340	0.1992	2.111
110	524	73.58	5	66.2	0.1002	1.883	0.1887	2.191	20	67.4	0.0839	2.340	0.1962	2.134
150	524	73.58	6	67.2	0.0867	2.060	0.1787	2.272	21	67.2	0.0866	2.340	0.2025	2.088
189	523	73.48	7	67.5	0.0815	2.190	0.1783	2.275	22	66.8	0.0908	2.340	0.2125	2.020
236	523	73.48	8	67.7	0.0787	2.270	0.1787	2.272	23	66.5	0.0950	2.340	0.2225	1.957
272	523	73.48	9	67.6	0.0803	2.315	0.1858	2.213	24	65.9	0.1032	2.340	0.2415	1.847
299	522	73.38	10	66.6	0.0925	2.330	0.2155	2.001	25	66.4	0.0954	2.340	0.2230	1.954
340	521	73.38	11	67.5	0.0804	2.335	0.1877	2.199	26	66.6	0.0924	2.340	0.2160	1.998
379	521	73.38	12	67.2	0.0844	2.340	0.1975	2.124	27	66.3	0.0965	2.340	0.2260	1.935
415	521	73.28	13	67.3	0.0817	2.340	0.1912	2.172	28	65.7	0.1034	2.340	0.2420	1.844
441	521	73.38	14	67.5	0.0804	2.340	0.1880	2.195	29	66.0	0.1005	2.340	0.2350	1.883
477	520	73.38	15	67.1	0.0856	2.340	0.2005	2.103	30	65.7	0.1048	2.340	0.2450	1.828
516	520	73.38	16	67.2	0.0844	2.340	0.1974	2.125	31	65.4	0.1088	2.340	0.2545	1.779
550	520	73.38	7	67.5	0.0804	2.190	0.1760	2.294	32	64.1	0.1264	2.340	0.2960	1.593

Barometer = 30.18 in.Hga. Pob = 30.76 in.Hga.; ΔP_{orf} = 4.60 in. H_2O
Average values at throat: ΔP = 35.7 in.Hg.; M = 1.022
Diffuser height = 1.718 in.

TABLE VI

Data Sheet for Shock Free Operation with Mach 2.37 Nozzle Blocks, Constant Diffuser Area and Increased Back Pressure

Time sec.	T_{o1} ^{o}R	P_{o1} in. Hg.a.	Tap No.	ΔP in. Hg.	P/P_{o1}	A/A*	$\left(\frac{P}{P_{o1}}\right)\left(\frac{A}{A^*}\right)$	M	Tap No.	ΔP in. Hg.	P/P_{o1}	A/A*	$\left(\frac{P}{P_{o1}}\right)\left(\frac{A}{A^*}\right)$	M
66	526	88.68	2	59.0	0.3350	1.097	0.3670	1.350	17	80.9	0.0877	2.340	0.2050	2.071
107	525	88.58	3	69.4	0.2160	1.340	0.2895	1.619	18	81.6	0.0787	2.340	0.1842	2.226
165	524	88.58	4	76.2	0.1396	1.621	0.2265	1.933	19	80.9	0.0866	2.340	0.2026	2.086
204	523	88.38	5	79.5	0.1004	1.883	0.1896	2.183	20	80.9	0.0846	2.340	0.1980	2.120
270	521	88.38	6	80.6	0.0879	2.060	0.1810	2.252	21	80.6	0.0879	2.340	0.2058	2.066
315	521	88.28	7	81.0	0.0825	2.190	0.1808	2.254	22	80.2	0.0914	2.340	0.2138	2.012
358	520	88.18	8	81.1	0.0802	2.270	0.1821	2.243	23	79.8	0.0950	2.340	0.2222	1.959
405	519	88.18	9	81.0	0.0814	2.315	0.1882	2.193	24	79.1	0.1029	2.340	0.2405	1.853
448	519	88.08	10	79.9	0.0977	2.330	0.2160	1.998	25	79.8	0.0940	2.340	0.2200	1.963
500	518	88.08	11	80.8	0.0825	2.335	0.1925	2.162	26	79.7	0.0951	2.340	0.2225	1.956
537	518	87.98	12	80.4	0.0662	2.340	0.2015	2.095	27	79.4	0.0975	2.340	0.2262	1.922
573	517	87.98	13	80.5	0.0850	2.340	0.1990	2.113	28	78.7	0.1055	2.340	0.2470	1.818
612	517	87.88	14	80.6	0.0828	2.340	0.1938	2.152	29	78.9	0.1022	2.340	0.2390	1.861
648	516	87.86	15	80.4	0.0851	2.340	0.1992	2.111	30	78.6	0.1057	2.340	0.2470	1.818
689	516	87.78	16	80.5	0.0829	2.340	0.1940	2.150	31	76.2	0.1091	2.340	0.2555	1.774
725	516	88.78	7	80.6	0.0817	2.190	0.1790	2.269	32	76.9	0.1238	2.340	0.2695	1.619

Barometer = 30.08 in. Hga. ; Pob = 38.98 in. Hga. ; ΔP_{orf} = 5.30 in. H_2O
Average values at throat: ΔP = 42.8 in. Hg. ; M = 1.022
Diffuser height = 1.718 in. Hg.

TABLE VII

Data Sheet for Shock Free Operation with Mach 2.37 Nozzle Blocks and Maximum Diffuser Area

Time sec.	T_{o1} ^{o}R	P_{o1} in. Hg.a.	Tap No.	ΔP in. Hg.	P/P_{o1}	A/A*	$\left(\frac{P}{P_{o1}}\right)\left(\frac{A}{A^*}\right)$	M	Tap No.	ΔP in. Hg.	P/P_{o1}	A/A*	$\left(\frac{P}{P_{o1}}\right)\left(\frac{A}{A^*}\right)$	M
90	525	74.68	2	49.7	0.3345	1.097	0.3665	1.352	17	68.1	0.0880	2.340	0.2060	2.064
131	525	74.68	3	58.4	0.2175	1.340	0.2910	1.613	18	68.6	0.0813	2.340	0.1902	2.179
171	525	74.68	4	64.1	0.1413	1.621	0.2293	1.916	19	68.1	0.0880	2.340	0.2060	2.064
217	525	74.58	5	67.0	0.1016	1.883	0.1915	2.169	20	68.2	0.0855	2.340	0.2000	2.106
261	525	74.58	6	68.0	0.0871	2.060	0.1795	2.265	21	67.9	0.0895	2.338	0.2092	2.042
287	525	74.58	7	68.3	0.0841	2.190	0.1842	2.227	22	67.7	0.0922	2.338	0.2155	2.001
319	524	74.58	8	68.4	0.0828	2.270	0.1879	2.197	23	67.3	0.0976	2.342	0.2287	1.920
367	524	74.48	9	68.4	0.0816	2.315	0.1888	2.190	24	66.7	0.1042	2.378	0.2388	1.862
397	523	74.58	10	67.7	0.0921	2.330	0.2145	2.011	25	67.8	0.0909	2.408	0.2190	1.979
434	523	74.58	11	68.4	0.0828	2.335	0.1933	2.155	26	68.1	0.0868	2.441	0.2120	2.023
465	523	74.58	12	68.1	0.0868	2.340	0.2030	2.085	27	68.2	0.0855	2.475	0.2093	2.041
494	522	74.58	13	68.2	0.0843	2.340	0.1973	2.126	28	67.8	0.0895	2.510	0.2245	1.945
530	522	74.58	14	68.3	0.0841	2.340	0.1970	2.128	29	67.8	0.0908	2.540	0.2305	1.909
559	521	74.48	15	68.1	0.0857	2.340	0.2005	2.103	30	68.0	0.0869	2.560	0.2223	1.958
589	521	74.48	16	68.2	0.0843	2.340	0.1973	2.126	31	68.1	0.0856	2.565	0.2195	1.975
677	521	74.48	7	68.2	0.0843	2.190	0.1845	2.223	32	66.9	0.1018	2.555	0.2600	1.753

Barometer = 30.08 in. Hga. ; Pob = 30.75 in. Hga. ; ΔP_{orf} = 4.70 in. H_2O
Average values at throat: ΔP = 36.2 in. Hg. ; M = 1.022
For diffuser areas see Table IV.

TABLE VIII

Data Sheet for Shock Free Operation with Mach 2.37 Nozzle Blocks and Minimum Diffuser Starting Area

Time sec.	T_{o1} ^{o}R	P_{o1} in. Hg.a.	Tap No.	ΔP in. Hg.	P/P_{o1}	A/A*	$\left(\frac{P}{P_{o1}}\right)\left(\frac{A}{A^*}\right)$	M	Tap No.	ΔP in. Hg.	P/P_{o1}	A/A*	$\left(\frac{P}{P_{o1}}\right)\left(\frac{A}{A^*}\right)$	M
79	525	61.78	2	41.3	0.3320	1.097	0.3640	1.359	17	56.3	0.0886	2.340	0.2075	2.053
142	524	61.78	3	48.3	0.2180	1.340	0.2920	1.606	18	56.6	0.0838	2.340	0.1960	2.135
197	524	61.68	4	52.4	0.1502	1.621	0.2440	1.835	19	56.3	0.0871	2.338	0.2035	2.083
248	524	61.68	5	55.4	0.1018	1.883	0.1919	2.166	20	56.3	0.0871	2.335	0.2035	2.083
286	524	61.58	6	56.1	0.0889	2.060	0.1831	2.235	21	56.1	0.0889	2.333	0.2073	2.053
325	523	61.58	7	56.3	0.0857	2.190	0.1878	2.198	22	55.8	0.0938	2.333	0.2185	1.982
365	523	61.58	8	56.5	0.0824	2.270	0.1870	2.204	23	55.6	0.0971	2.308	0.2242	1.947
382	523	61.58	9	56.5	0.0824	2.315	0.1908	2.176	24	54.7	0.1115	2.262	0.2522	1.791
412	523	61.58	10	56.1	0.0889	2.330	0.2072	2.056	25	54.5	0.1148	2.215	0.2542	1.781
438	523	61.58	11	56.4	0.0840	2.335	0.1960	2.135	26	53.8	0.1261	2.165	0.2730	1.691
467	523	61.48	12	56.1	0.0875	2.340	0.2048	2.072	27	53.2	0.1347	2.115	0.2843	1.641
496	522	61.48	13	56.2	0.0859	2.340	0.2010	2.099	28	53.0	0.1378	2.090	0.2878	1.626
536	522	61.48	14	56.4	0.0826	2.340	0.1932	2.156	29	51.4	0.1639	1.980	0.3245	1.485
568	522	61.48	15	56.2	0.0859	2.340	0.2010	2.099	30	51.3	0.1653	1.943	0.3220	1.494
591	522	61.48	16	56.2	0.0859	2.340	0.2010	2.099	31	51.6	0.1605	1.920	0.3080	1.545
620	522	61.38	7	56.2	0.0845	2.190	0.1850	2.220	32	49.4	0.1952	1.908	0.3721	1.345

Barometer = 30.08 in.Hga. ; P_{ob} = 30.53 in. Hga. ; ΔP_{orf} = 3.15 in. H_2O
Average values at throat: ΔP = 38.38 in. Hg. ; M = 1.022
For diffuser areas see Table III.

TABLE IX
Data Sheet for Shock-in-Nozzle Operation with
Mach 2.37 Nozzle Blocks and Constant Diffuser Area

Time Secs.	T_{o1} °R	P_{o1} in. Hg.a.	TAP NO.	P in. Hg.	P/P_{o1}	TAP NO.	P in. Hg.	P/P_{o1}
873	519	63.28	2	42.3	0.3320	17	39.8	0.3720
907	519	63.18	3	49.7	0.2130	18	39.4	0.3765
950	519	63.18	4	54.6	0.1358	19	38.8	0.3860
993	519	63.18	5	49.8	0.2110	20	37.8	0.4020
1032	519	63.08	6	49.7	0.2115	21	37.0	0.4130
1065	519	63.08	7	48.5	0.2305	22	36.5	0.4210
1095	519	63.08	8	46.9	0.2560	23	35.9	0.4300
1135	519	63.08	9	44.6	0.2920	24	35.5	0.4375
1165	519	63.08	10	42.5	0.3280	25	35.4	0.4390
1196	519	63.08	11	41.5	0.3420	26	35.3	0.4400
1225	519	63.08	12	39.2	0.3780	27	35.2	0.4420
1258	519	62.98	13	39.5	0.3735	28	35.2	0.4420
1289	519	62.98	14	39.9	0.3670	29	35.3	0.4400
1343	519	62.88	15	39.7	0.3680	30	35.3	0.4390
1383	519	62.88	16	39.7	0.3680	31	35.4	0.4375
1412	519	62.88	7	48.3	0.2315	32	35.4	0.4375

Barometer = 30.18 in. hge. ; P_{ob} = 30.69 in. hge; ΔP_{orf} = 3.45 in. H_2O

Averege values at throat: ΔP = 30.7 in. hg.; M = 1.025

Diffusar height = 1.718 in.

TABLE IX - Cont'd

TAP Number	A/A_x^*	$\frac{P}{P_{o1}} \frac{A}{A_x}$	M	$\frac{P}{P_{oy}}$	$\frac{P_{oy}}{P_{o1}}$
2	1.097	0.364	1.359	0.3328	-----
3	1.340	0.286	1.635	0.2233	-----
4	1.621	0.220	1.970	0.1339	-----
5	1.883	0.398	1.265	0.3784	0.558
6	2.060	0.436	1.175	0.4260	0.496
7	2.190	0.505	1.038	0.5051	0.457
8	2.271	0.581	0.921	0.5778	0.444
9	2.315	0.676	0.805	0.6528	0.448
10	2.330	0.765	0.702	0.7196	0.456
11	2.335	0.799	0.690	0.7274	0.470
12-18	2.340	0.867	0.642	0.7579	0.489
19	2.340	0.902	0.620	0.7716	0.500
20	2.340	0.941	0.594	0.7877	0.511
21	2.340	0.965	0.581	0.7956	0.519
22	2.340	0.985	0.568	0.8034	0.524
23	2.340	1.005	0.560	0.8082	0.532
24	2.340	1.023	0.549	0.8148	0.537
25	2.340	1.026	0.548	0.8153	0.538
26	2.340	1.029	0.546	0.8165	0.539
27	2.340	1.034	0.544	0.8177	0.541
28	2.340	1.034	0.544	0.8177	0.541
29	2.340	1.029	0.546	0.8165	0.539
30	2.340	1.026	0.548	0.8153	0.538
31	2.340	1.023	0.549	0.8148	0.537
32	2.340	1.023	0.549	0.8148	0.537

APPENDIX A

TUNNEL SYSTEM OPERATION PROCEDURE

I. For charging the storage tanks the following procedure should be followed:

1. Open the 3/4 inch valve connecting the trap with the separator.
2. Close the 3/4 inch drain valve located below the tee after the trap.
3. Open the 1/4 inch balance line valve between the separator and the trap.
4. Open the cooling water valve to the after-cooler heat exchanger.
5. Close both two inch inlet valves located at the entrance to the low pressure storage tanks.
6. Open the valve on the low pressure after-cooler.

NOTE: Items 5 and 6 are safety precautions to prevent high pressure air from entering the low pressure tanks.

7. Close the drain valve on each high pressure tank.
8. Close the two inch discharge valve on each high pressure tank outlet.
9. Open the inlet valve to each high pressure tank.
10. Place the unloader on the compressor in the START position (vertical with the index head down.)
11. Place cover on the compressor oil vent.
12. Open the air supply valve to the Bailey controller (Pressure should read 28 psi).

13. Adjust compressor discharge pressure for a pressure slightly higher than any pressure indicated in the receivers. This is done by turning the adjustment knob on the Bailey Controller counterclockwise until the red hand indicates the desired pressure.

14. Connect the cooling air circulating centrifugal blower in the compressor shack.

15. Throw the master power switch located in the main bulkhead switch panel for the High Pressure Air Compressor to the ON position.

16. In the compressor shack, throw the overload trip arm to the ON position and push the START button.

17. After the compressor has started running, place the unloader valve in the RUN position (handle horizontal with the index head pointing towards the compressor.)

18. Adjust the compressor discharge pressure regulator valve to give the desired discharge pressure. (Maximum 500 psi)

19. Maintain a check on the storage tank pressure as an automatic unloader for the compressor is not provided.

20. Should an excess amount of air be coming out of the drain line from the trap, it is probable that additional water is required in the trap. Water may be added when the compressor is secured through the union connection of the balance line until it is observed coming out of the trap drain.

21. To secure the compressor place the unloader valve in the START

position, push the STOP button and remove the oil vent cover. An emergency STOP button is also located with the Bailey controller.

22. Close the inlet valves to the storage tanks.
23. Close the balance line valve.
24. Close the valve connecting the separator and trap.
25. Close the air supply valve to the Bailey Controller.
26. Blow down excess air in the lines from the compressor to the storage tank inlet valves by opening the trap drain valve.
27. Secure the cooling water.
28. The drain on each high pressure tank and the inner cooler should be blown at periodic intervals to remove any accumulation of oil or water.

position, push the STOP button and remove the oil vent cover. An emergency STOP button is also located with the Bailey controller.

22. Close the inlet valves to the storage tanks.
23. Close the balance line valve.
24. Close the valve connecting the separator and trap.
25. Close the air supply valve to the Bailey Controller.
26. Blow down excess air in the lines from the compressor to the storage tank inlet valves by opening the trap drain valve.
27. Secure the cooling water.
28. The drain on each high pressure tank and the inner cooler should be blown at periodic intervals to remove any accumulation of oil or water.

II. Blow down procedure

1. Open the outlet valves on each high pressure tank.
2. Open the air supply valve to the stagnation pressure Bailey Controller (Supply pressure should read 28 psi).
3. Open the quick opening valve at the outlet of the regulator valve.
4. Slowly turn the adjusting knob of the Bailey controller counter clockwise to allow a gradual buildup of pressure in the stilling tank to the desired stagnation pressure. A loading pressure of at least 5 psi is required before the regulator valve will open.
5. Figure 1-A gives the approximate differential pressure required to obtain the maximum Mach number in the tunnel test section for a given stagnation pressure measured above atmospheric pressure in inches of mercury.
6. The time of each run may be prolonged as well as reducing the rate of change of stagnation temperature by allowing the compressor to continue charging the storage tanks while operating the tunnel.

FIG. 1-A. PRESSURE DIFFERENTIAL BETWEEN STAGNATION PRESSURE AND TUNNEL TEST SECTION PRESSURE REQUIRED TO OPERATE TUNNEL AT MACH 2.971 VS STAGNATION PRESSURE.

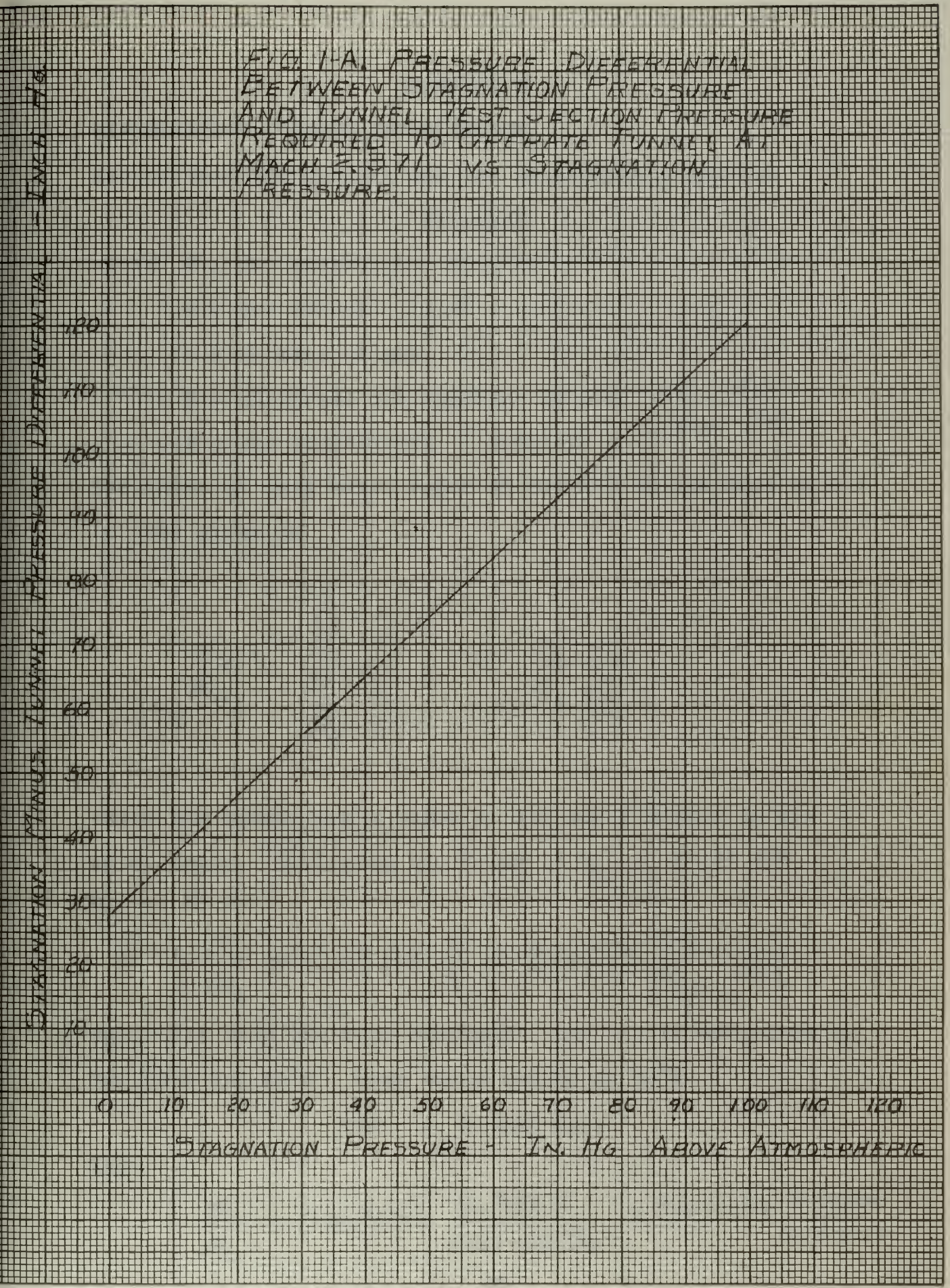

APPENDIX B

AIR MOISTURE CONTENT CALCULATIONS.

Assume that the perfect gas law relationship applies

$$PV = mRT$$

where P = gas pressure lb_f/ft^3

V = gas volume ft^3

m = lb mass of gas

R = universal gas constant of gas, $\frac{ft - lb_f}{lb_m - {}^\circ R}$

T = gas temperature, $^\circ$ Rankine.

The ratio of mass water vapor in the air to the mass of air is then given by

$$\frac{m_v}{m_a} = \frac{\frac{P_v}{R_v}\frac{V}{T}}{\frac{P_a}{R_a}\frac{V}{T}} = \frac{R_a}{R_v}\frac{P_v}{P_a}$$

where the subscripts a refer to air and v refers to the water vapor. Utilizing the value of R_a = 53.34 and R_v = 85.7

$$\frac{m_v}{m_a} = 0.6225\,\frac{P_v}{P_a} = 0.6225\,\frac{P_v}{P_{TOTAL} - P_v}$$

Upon exit from the heat exchanger, the air is saturated at 500 psia and 60°F. From steam tables at 60°F

Psat = 0.2563 psia

and

$$\frac{m_v}{m_a} = 0.6225 \times \frac{0.2563}{500 - 0.2563} = 0.000319\ \frac{lb\ vapor}{lb.\ dry\ air}$$

APPENDIX C

FLOW RATE CALCULATION PROCEDURE.

The mass rate of flow for the tunnel, as measured at the orifice plate, was determined by the procedure outlined by the American Society of Mechanical Engineers [5]. All equations, figures or table numbers correspond to numbers in that publication. Due to the removal of the water vapor by the air drying system, it is assumed the air is dry for metering purposes. In addition, due to the low velocity of the air, the air is considered incompressible.

For a representative run:

P_{ol} = 72.08 in. Hg.

T_o = 525°R = 25°F

P_{ob} = 30.84 in. Hg.

D = Pipe diameter = 3.120 inches.

d = 2.496" = orifice diameter

$\beta = \frac{\text{orifice diameter}}{\text{pipe diameter}} = \frac{d}{D} = 0.800$

ΔP = differential pressure in inches of H_2O = 4.55

Equation 2, page 57, gives the mass rate of flow lbm/hr.

$$\dot{m} = 359 C F d^2 F_a \sqrt{h_w \gamma}$$

Where C = coefficient of discharge

F = velocity of approach factor

F_a = thermal expansion factor

h_w = differential pressure in inches of H_2O

γ = specific weight of air at the inlet side of the primary element, lb/ft^3

From Figure 38, page 67, for a stainless steel orifice plate at 65^oF

Fa = 1.00

From Table 9, page 80, at 65^oF

$\gamma_{air} = 0.075650\ lb/ft^3$ at 29.92 in. Hg.

Correcting for increase in pressure

$$\gamma_{air} = 0.07565 \times \frac{30.84}{29.92} = 0.0762\ lb/ft^3$$

$d^2 = (2.496\ in.)^2 = 6.230\ in.^2$

Assume a value of K = CF = 0.80 and calculate an approximate $\dot{m}$

$$\dot{m} = 359 \times 0.800 \times 6.230 \sqrt{4.55 \times 0.0762}$$

$$= 1053\ lbm/hr.$$

And $g\mu$ from Figure 35, page 62, for 65^oF air = .0000122

Calculate Reynolds number R_D from Equation 8.

$$R_D = \frac{0.004244\ \dot{m}}{Dg\mu} = \frac{0.004244 \times 1053}{3.120 \times 0.0000122} = 117{,}600$$

From Table 5, page 26, or from Figure 1-C of this Appendix, for β = 0.800, and R_D = 117,600 the flow coefficient is K = 0.8062

Corrected calculation of flow rate, therefore is

$$\dot{m} = 359 \times 0.8062 \times 6.230 \sqrt{4.55 \times 0.0762}$$

$$= 1060\ lbm/hr. = 0.2945\ lbm/sec.$$

The ideal mass flow rate at the nozzle throat is determined by Fliegner's formula [2].

$$\dot{m}_i = 0.532 \frac{A^* P_o}{\sqrt{T_o}}$$

Where $\dot{m}_i$ = ideal flow rate lbm/sec.

A^* = tunnel throat area in square inches with M = 1.00 .

P_{o_1} = stagnation pressure psia

T_{o_1} = stagnation temperature in ^{o}Rankine

$$\dot{m}_i = \frac{0.532 \times 0.367 \times 72.08 \times 0.491}{\sqrt{525}}$$

$$= 0.301 \text{ lbm/sec.}$$

The nozzle discharge coefficient C_D is defined as the ratio of the actual nozzle flow to the flow calculated from the isentropic laws for the initial and final pressures of the actual nozzle. Based on this definition the coefficient of discharge is

$$C_D = \frac{\dot{m}_{actual}}{\dot{m}_{ideal}} = \frac{0.2945}{0.301} = 0.969$$

Figure 1-C presents the Flow Coefficient K plotted vs. the Reynolds Number for a flat plate orifice with pressure taps at D and 1/2 D for a three inch pipe. This figure presents the data of Table 5 (5) graphically for values of d/D equal to 0.580 and 0.800. Figure 25 presents graphically the nozzle discharge coefficient C_D plotted vs. the stilling tank stagnation pressure. Values of C_D were determined by the use of Fliegner's formula and by the

procedure outlined by the American Society of Mechanical Engineers (5) as used in this Appendix.

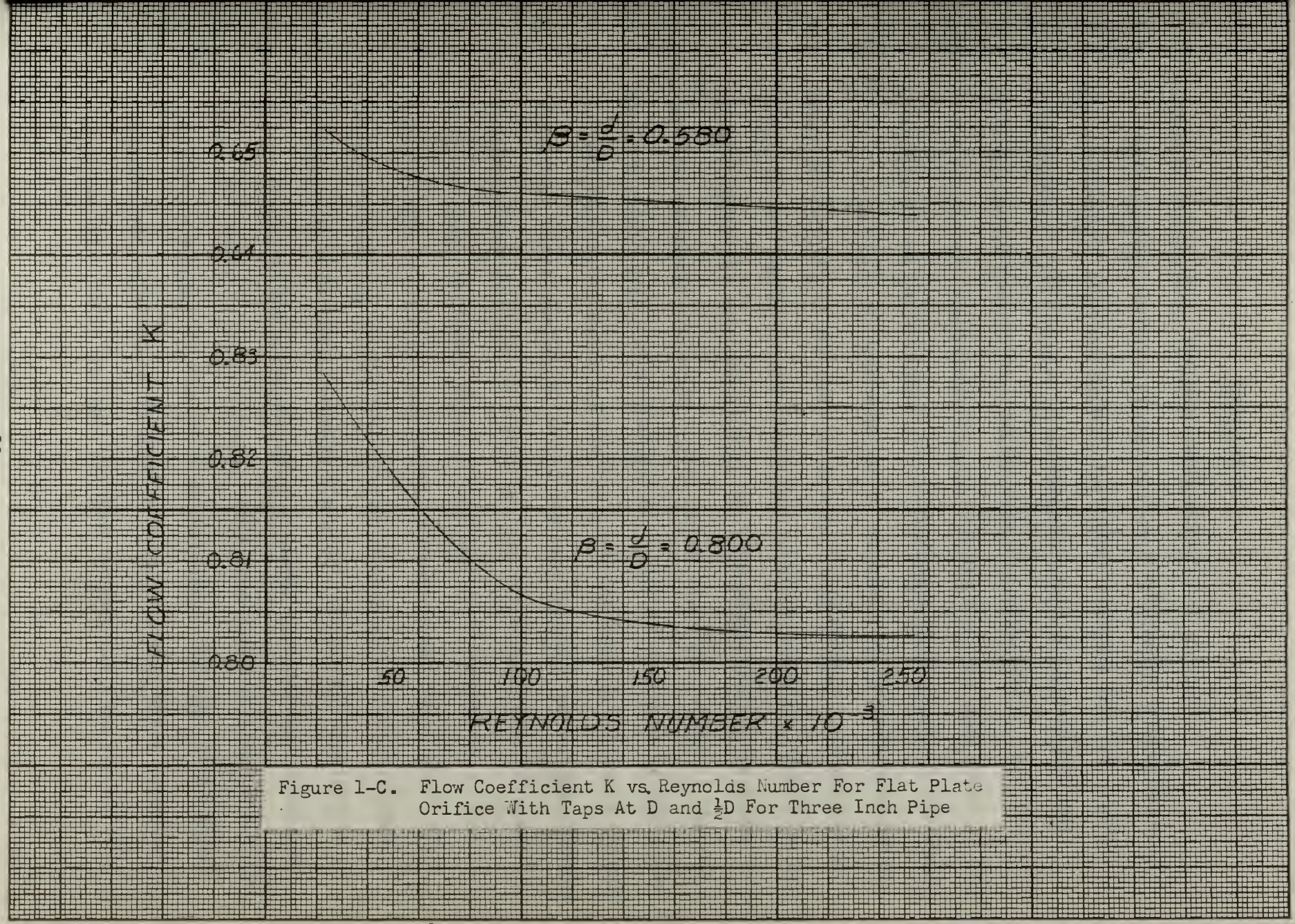

Figure 1-C. Flow Coefficient K vs. Reynolds Number For Flat Plate Orifice With Taps At D and $\frac{1}{2}$D For Three Inch Pipe

APPENDIX D

DESIGN OF DIFFERENTIAL PRESSURE TRANSDUCER.

Differential pressure transducers were originally to have measured the differential pressure between the tunnel pressure and the stagnation pressure. This method of measurement was discarded due to the difficulties of fabricating similar output transducers.

A successful transducer, Figures 2-D and 3-D, was made based on the principle of the deflection of a circular plate held firmly at the edge [14]. It was desired that each psi of differential pressure produce at least 10 microinches per inch of strain. Transforming the equation of stress at the center of the clamped plate to the equation of strain (end of this appendix) and substituting the appropriate values, the plate thickness was calculated as being 0.0336 inches times the radius of the plate. One A-7 strain gage was located at the center of each side of the plate and the cumulative output of the two gages was read on a Baldwin strain indicator. This cumulative output was thus expected to be approximately 20 microinches per inch of strain per psi of differential pressure.

The plate thickness actually used was 0.032 inches due to the availability of this uniform thickness sheet stock. This plate was welded between two hollow cylinderical shells of 1.5 inches inside diameter and 2.25 inches outside diameter. While this combination of plate thickness and effective plate diameter exceeded the calculated plate thickness to plate diameter ratio, the combined output still exceeded the desired minimum of 10 microinches. The open ends of the cylinderical shells were threaded to receive a plug which contained a pressure tap. An O-ring seal was used between the plug and the shell

of the transducer.

One leg of each strain gage was led through the shell wall and the drilled hole secured with epoxy cement. The other leg of the gage was soldered to the inside of the shell which served as a common ground between the two gages. The two protruding wires from the gages and a common ground wire, soldered to the outside of the shell, were then connected to the Baldwin strain gage indicator.

The completed transducer was calibrated on a hydraulic dead weight tester. One end of the transducer was vented to the atmosphere and the other cavity filled with oil and connected to the dead weight tester. A pressure differential ranging from 0 to 100 psi, in increments of 10 pounds, was then imposed with strains recorded while loading and unloading the tester.

A linear plot of pressure differential vs. strain was obtained for several transducers but on others, the welding caused a slight permanent buckle in the plate and the strain indications were not reproduceable for a given pressure differential. Due to the time involved in making and testing each transducer, it was felt that too much unproductive time would be spent on making transducers that could not be used; so this means of pressure measurement was abandoned in favor of manometer pressure measurements.

One test transducer was glued together with Eastman 910 glue to eliminate the problems caused by the buckling of the diaphragm due to welding. A centering hole and shoulder was made in the cylinderical shells, the diaphragm was then glued to both shells under light pressure.

The strain gages were attached to each side of the diaphragm prior to joining the two end shells. This transducer gave a linear plot of 18.52 microinches per inch of strain/psi of pressure differential when tested on the hydraulic dead weight tester but it did not respond to less than 3/4 of an inch of mercury pressure differential when checked against a manometer reading of the same pressure differential with the tunnel in operation.

The stress distribution in a uniformly loaded diaphragm with clamped edges is given in Figure 1-D below [14].

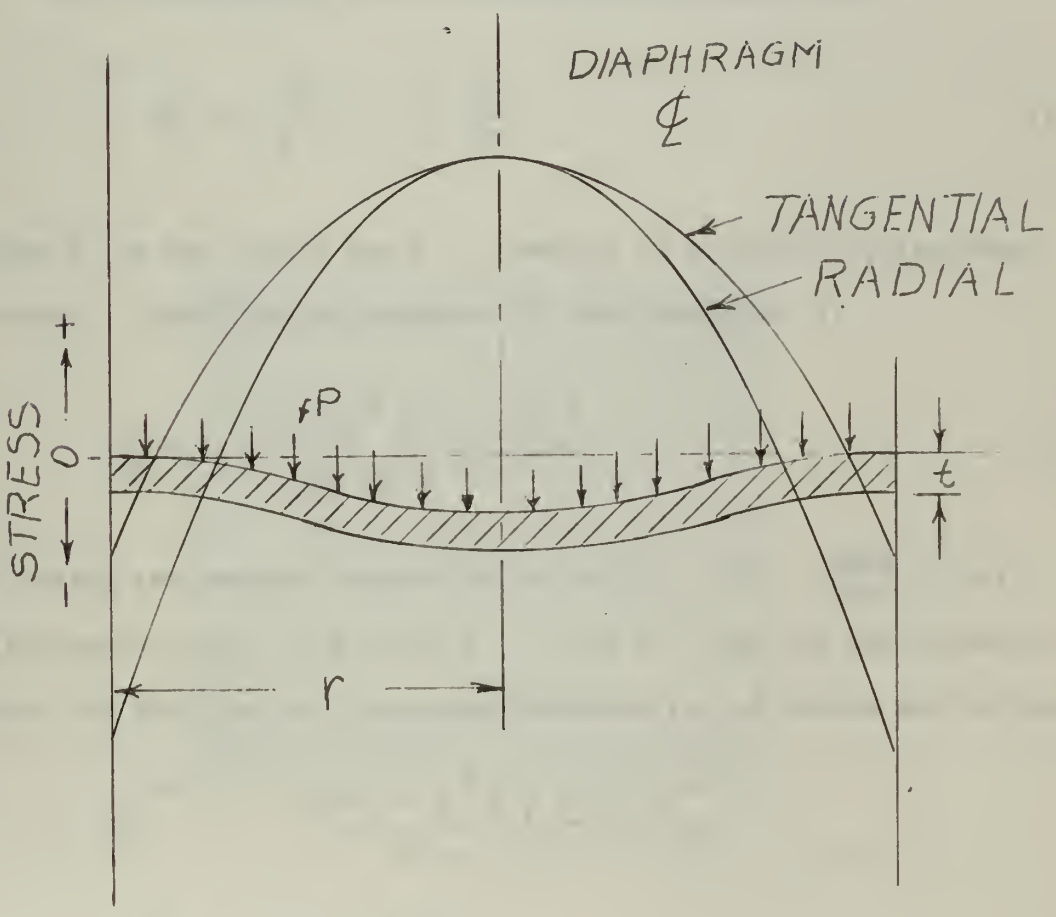

Figure 1-D Stress Distributions of Diaphragm

The tangential stress at the center of the plate is given by the equation

$$S = \frac{3(1+\mu)Pr^2}{8t^2} \qquad (1)$$

Where S = stress in psi.

μ = Poisson ratio.

P = Pressure differential in psi.

r = Radius of diaphragm in inches.

t = Diaphragm thickness in inches.

The corresponding value of strain is obtained from

$$\epsilon = \frac{S}{E} - \mu\frac{S}{E} \qquad (2)$$

where ϵ is the strain and E = modulus of rigidity of diaphragm material. Substituting equation (2) into equation (1)

$$\epsilon = \frac{3Pr^2(1-\mu^2)}{8Et^2} \qquad (3)$$

Utilizing the required minimum value of $\epsilon = 10^{-5}$ $\frac{\text{inch}}{\text{inch}} / \text{psi}$ differential, $\mu = 0.3$ and $E = 30 \times 10^6$ psi for the values of steel the ratio of the diaphragm thickness to its radius may be obtained.

$$10^{-5} = \frac{3 \times 1 \times r^2(1-0.3^2)}{8 \times 3 \times 10^7 \times t^2}$$

$$\frac{t}{r} = 0.0336 \qquad (4)$$

For a diaphragm radius of 0.75 inches a plate thickness of 0.0252 inches is required.

Figure 2-D. Exterior View of Welded Pressure Transducer.

Figure 3-D. Interior View of Welded Pressure Transducer.

APPENDIX E

GENERAL THEORY OF THE SCHLIEREN METHOD OF OPTICAL INVESTIGATION OF COMPRESSIBLE FLUID FLOW [2].

Apart from the conventional methods of experimentally investigating flow patterns by means of pressure and velocity surveys, compressible gas flows lend themselves particularly well to optical methods of investigation.

Fundamentally, the optical methods in common use (the interferometer, the Schlieren, and the shadowgraph) depend on one of the two physical phenomena: (1) the speed of light depends on the index of refraction of the medium through which it passes, and the index of refraction of a gas in turn depends upon its density; and, as a consequence of this first phenomenon, (2) light passing through a density gradient in a gas (and therefore through a gradient in index of refraction) is deflected in the same manner as though it were passing through a prism. In a high-speed gas flow the density changes are sufficiently large to make these phenomena sizeable enough for optical observation.

The interferometer, based on phenomenon (1), measures directly changes of density, and is primarily suited for quantitative determination of the density field.

The Schlieren method, based on phenomenon (2), measures density gradients. Although it is theoretically adaptable to quantitative use, it is inferior to the interferometer in this respect, and its greatest utility is in giving an easily interpretable picture of the flow field

together with a rough picture of the density variations in the flow.

The shadowgraph method, also based on phenomenon (2), measures the second derivative of the density (i.e., the first derivative of the density gradient). Therefore it makes visible only those parts of the flow where the density gradients change very rapidly, and it has found its greatest utility in the study of shock waves.

Of the three methods mentioned, the interferometer yields the most information, and the shadowgraph the least. On the other hand, the interferometer is the most costly and the most difficult to operate, whereas the shadowgraph is the least costly and the easiest to operate. Each method therefore has its own useful niche in experimental work, and the choice of method depends on the nature of the investigation.

Figure 1-E below shows one of the numerous type of Schlieren (striae) arrangements. Light from a uniformly illuminated line source

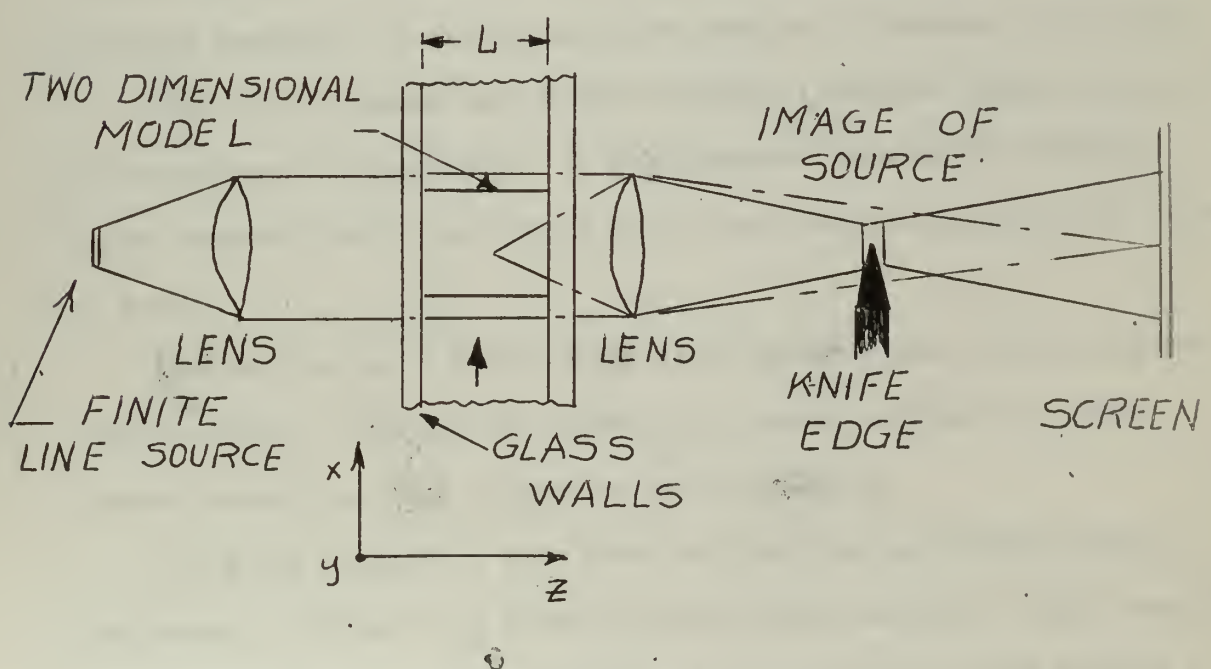

Figure 1-E Schematic Schlieren System

of small but finite width is collimated by the first lens and then passes through the test section. It is then brought to a focus by the second lens and projected on the screen. At the focal point, where there exists an image of the source, there is introduced a knife-edge which cuts off part of the light. With no flow in the test section the knife-edge is usually adjusted so as to intercept about half the light, and the screen is uniformly illuminated by the portion of the light escaping the knife-edge. When the flow is established in the test section assumed, for simplicity, to be two dimensional, with each light ray passing through a path of constant air density any light ray passing through a region in which there is a density gradient normal to the light direction will be deflected as though it has passed through a prism. Therefore, depending on the orientation of the knife-edge with respect to the density gradient, and on the sign of the density gradient, more or less of the light passing through each part of the test section will escape the knife-edge and illuminate the screen.

Thus the Schlieren system makes density gradients visible in terms of intensity of illumination. A photographic plate at the viewing screen records density gradients in the test section as different shades of gray.

For the Schlieren figure drawn it is assumed that the flow in the test section is parallel and in the x, y-plane, and that the light passes through the test section in the z-direction.

Since the speed of a wave front of light varies inversely with the index of refraction n of the medium through which the light travels, it follows that a given wave front will rotate as it passes through a gradient in n. Accordingly, the normal to the wave front will follow

a curved path; since this normal is what we mean by the light ray, the latter is refracted as it passes through the density gradient. Noting that n is nearly unity for gases, it may be shown that

$$\frac{1}{R} = \text{gradient } n$$

where R is the radius of curvature of the light ray. The total angular deflection ε of the ray in passing through the test section of width L is therefore given by

$$\varepsilon = \frac{L}{R} = L \text{ grad } n$$

Resolving this into Cartesian components, and connecting the index of refraction with the gas density through the empirical Gladstone-Dale equation which states that

$$\frac{n-1}{\rho} = K_{G-D}$$

where K_{G-D}, the Gladstone-Dale constant, is constant for a given gas, we get the angular deflections of the light in the x- and y-directions

$$\varepsilon_x = L \frac{\partial n}{\partial x} = L K_{G-D} \frac{\partial \rho}{\partial x}$$

$$\varepsilon_y = L \frac{\partial n}{\partial y} = L K_{G-D} \frac{\partial \rho}{\partial y}$$

If the knife-edge is aligned in the y-direction (i.e., normal to the flow) as in Figure 1-E, only deflection in the x-direction will influence the light passing the knife-edge. Hence density gradients in the x-direction will be

made visible, but gradients in the y-direction will not be visible. Similarly, if the knife-edge is parallel to x, only gradients in the y-direction will become visible.

In interpreting a Schlieren photograph of a two dimensional flow, it is convenient to imagine that the photograph represents a view of a relief map of the flow field in which the vertical elevation is the gas density. If the map is illuminated by glancing side light nearly parallel to x, the pattern of shadows and brightness will correspond to a Schlieren photograph with the knife-edge in the y-direction. Similarly, illumination in the y-direction corresponds to placing the Schlieren knife-edge parallel to the x-direction.

Figures 14b and 14c are Schlieren photographs of the installed test section and show the two different effects obtainable with orientations of the knife-edge. In Figure 14b (knife-edge horizontal) light areas on the upper half correspond to dark areas on the lower half, and vice versa; the boundary layers on the walls are clearly visible, since with this knife-edge orientation the density gradients normal to the flow are made visible. In Figure 14c (knife edge vertical) the upper and lower halves look alike; the boundary layers are not visible, except aft of the shock wave which is inneracting with the boundary layer.

The quality of focus of the Schlieren pictures is believed to be poor due in part to the present arrangement of the Schlieren system installed for the reasons as outlined below by Holder and North [7]:

Although it is usually desirable to arrange for the

beam of light passing through the working section to be parallel, nonparallel beams are occasionally used and an arrangement for producing this type is sketched in Figure 2-E. Only one mirror or lens is required (apart from the focussing lens), but this advantage is to some extent offset because its diameter must be larger in relation to the field to be examined than if a parallel beam is used.

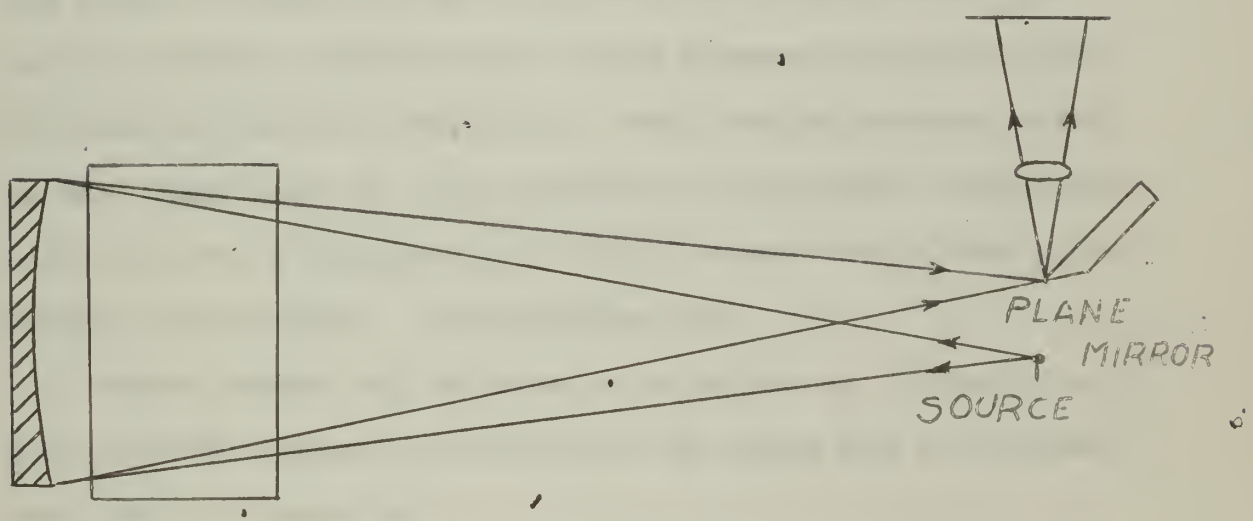

Figure 2-E. Coincidence Schlieren System using a Plane Mirror or knife-edge

In addition to employing a nonparallel light beam, the mirror system involves a double passage of the beam across the working section. The source is placed at the center of curvature of the mirror, and part of the image of the source is reflected on to the viewing screen by a small plane mirror held near the source. Because the

source and its image are very close to each other, the arrangement is often referred to as the "coincidence" system. If the image of the source is deflected in a direction perpendicular to the edge of the plane mirror, the illumination on the viewing screen changes; the edge of the mirror thus plays the same part as the knife edge in a Toepler apparatus.

Since the source and its image are not truly coincident, the paths of the incident and reflected rays across the working section differ even in the absence of deflections produced by density gradients. This has an adverse effect on the image quality (in addition to any effect associated with the use of non-parallel light) since two slight offset images are produced. (See Figure 16c)

These images may be made to coincide at the expense of considerably reduced illumination by using the arrangement sketched in Figure 3-E.

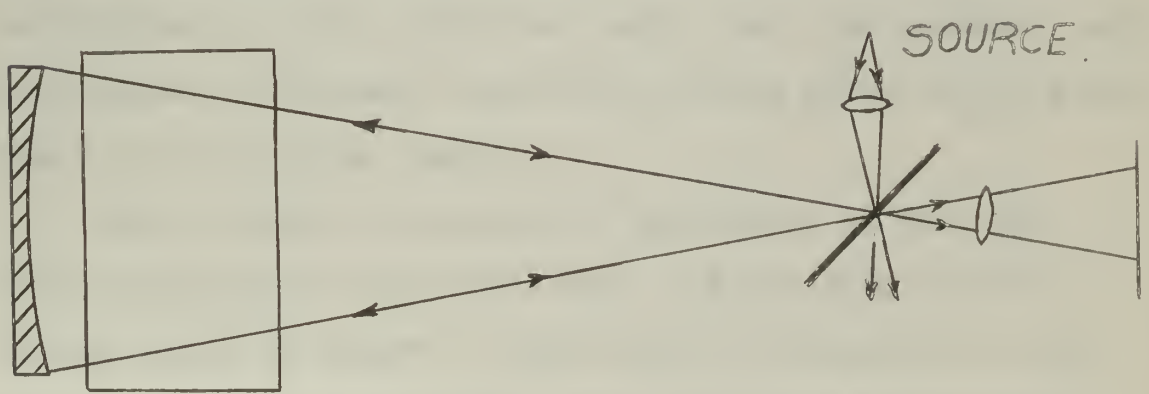

Figure 3-E. Coincidence Schlieren System using Graded Filter

Here a graded filter is placed at 45 degrees to the axis at the center of curvature of the mirror. A condenser lens is used to produce an image of the source on the surface of the filter, and part of the light from this image is reflected into the mirror. The image of the source formed by reflection from the mirror is made to coincide with the original image on the surface of the filter, and the light transmitted by the filter is arranged to fall on the viewing screen in the usual way. The source and its image may thus be made exactly coincident so that, in the absence of density gradients, the incident and reflected beams coincide. This will no longer be the case when the rays are deflected by density gradients, and some loss of image sharpness, or difficulty in interpreting the observations, may then result.

A further difficulty arises because only one of the two images formed by the incident and the reflected light can be in focus. It is usually best to focus the image associated with the reflected light since the incident rays are subject to further refraction during their second passage across the wind tunnel.

The principal advantage of the system is that the double passage of the light beam, and the fact that the source image is formed at the center of curvature of the mirror instead of its focus, give increased sensitivity. For example, in a two-dimensional flow containing a region of density gradient of sufficient extent for the incident and reflected ray to remain within it, the

angular deflection of the ray will be doubled by the use of such a system. Moreover, the displacement of the image of the source for a given angular deflection will be twice as large when the image is at the center of curvature as when it is at the focus. Coincidence systems may thus be valuable where extreme sensitivity is required (for example, tunnels working with very low density), although for ordinary use they are undesirable for the reasons mentioned above.

Part of the increased sensitivity associated with a double-passage system may be retained, without the difficulties associated with the use of non parallel light by means of the arrangement sketched in Figure 4-E. Here a parallel beam of light is produced by a lens or mirror and after crossing the working section it is reflected back by means of a plane mirror.

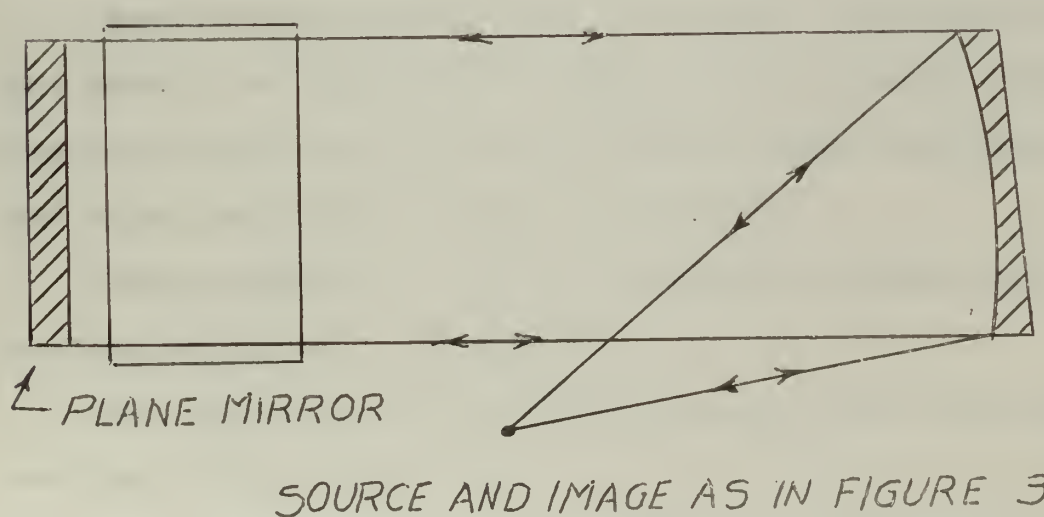

Figure 4-E. Schlieren System with Parallel Light Beams Crossing Tunnel Twice with Increased Sensitivity.

angular deflection of the ray will be doubled by the use of such a system. Moreover, the displacement of the image of the source for a given angular deflection will be twice as large when the image is at the center of curvature as when it is at the focus. Coincidence systems may thus be valuable where extreme sensitivity is required (for example, tunnels working with very low density), although for ordinary use they are undesirable for the reasons mentioned above.

Part of the increased sensitivity associated with a double-passage system may be retained, without the difficulties associated with the use of non parallel light by means of the arrangement sketched in Figure 4-E. Here a parallel beam of light is produced by a lens or mirror and after crossing the working section it is reflected back by means of a plane mirror.

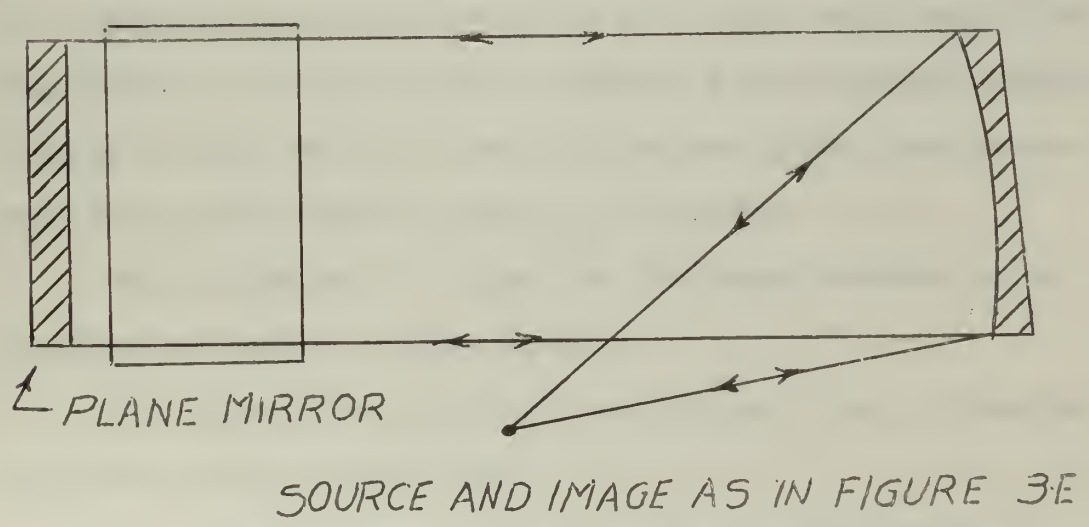

Figure 4-E. Schlieren System with Parallel Light Beams Crossing Tunnel Twice with Increased Sensitivity.

Tinsley Laboratories Inc. furnished the basic components for the coincidence Schlieren system as well as the design as shown in Figure 11. One unit was the six inch spherical mirror with a focal length of 80 inches mounted on a small pedestal. The other unit, mounted on a wooden frame with leveling jacks, consisted of the light source, knife edge, surface mirror and encased in a light tight wooden box the camera lens, folding surface mirrors and a six inch ground glass view plate. These were mounted on a portable stand as shown in Figure 9.

An Ilex Optical Company Number 3 Acme Synchro Shutter was installed between the knife edge and the camera lens by means of a machined adapter fitted over the lens mounting with the shutter bolted to it. This arrangement allowed all of the light passing over the knife edge to enter the camera lens system but otherwise maintained the light tight integrity of the system.

The six inch ground glass view plate was removed and the back of an Ilex Optical Company Korona camera consisting of a four inch by five inch ground glass view plate and film pack holder fitted in its place.

The procedure to align the Schlieren system is as follows referring to Figure 11:

1. Locate the spherical mirror as close to the test section window as practical.

2. Locate camera, light source, and knife-edge assembly such that the light source lies on an axis

perpendicular to the window. The light source should be approximately 80 inches from the spherical mirror surface. This may be done by moving the spherical mirror in the slots provided on the stand.

3. With the light source "turned-On" adjust the spherical mirror to image the light source at the knife-edge. If the image is not in focus with the knife-edge assembly at approximately the middle of its slide travel, move the spherical mirror forward or back to correct the image focus. (A small black card is helpful in locating images and the light beam directions.)

4. Adjust the knife-edge screw such that the "Knife" does not intercept the light source image. The light should then pass through the camera lens, and an image of the test region should appear on the view screen. If the view screen image is not centered, adjust the small 1st surface mirror and the spherical mirror such that the light passes through the center of the camera lens and aperture of the knife-edge assembly. If the view screen image is yet not centered, adjustment of the three small screw heads at the back of the camera will provide the final centering adjustment.

5. The knife-edge can now be freely adjusted to provide the required Schlieren sensitivity.

NOTE: All mirrors are front surface aluminized and should not be touched on the reflecting surface. They should be cleaned by dusting with a quality camels hair brush.

The best photographs of the flow field were obtained using the following camera settings:

1. Shutter speed set at 1/200 of a second.
2. Lens opening at f-11. This value has nothing to do with the actual exposure time of the film. This value of the lens opening allows all of the light beam to enter the camera and helps reduce stray light entering the lens system and fogging the film.
3. Royal Pan film with a tungsten film speed rating of 160 was used.
4. Developing time of eight minutes in total darkness in a 1 : 1 dilute mixture of Eastman DK 50 developer and water at 68^{o}F.

Colored Schlieren views of the flow field may be obtained by replacing the knife-edge assembly with the color grid purchased from Tinsley Laboratories. Colored pictures were not attempted as a means of printing and developing the color film was not available.

The light source may be either a General Electric Company bulb number 1968 or number 1924, or a Westinghouse bulb number 1633. All three bulbs produce a line source of light. If the General Electric bulbs are used, a different mount must be made for the bulb.

Both the light source and the knife edge may be rotated from the horizontal position to the vertical position to obtain the desired direction of the density gradient of the flow field.

For the reasons already outlined, the focus of this Schlieren system is not as sharp as could be obtained with a two mirror one pass light beam system.

A metal frame was fitted over one of the Schlieren windows and small copper wires were soldered into position at one inch intervals, starting at the throat position, to give horizontal dimensions.

APPENDIX F

SAMPLE CALCULATIONS FOR EXPERIMENTAL DATA AND THEORETICAL PREDICTIONS.

PREDICTION OF ADIABATIC MACH NUMBERS FOR NOZZLE AND CONSTANT AREA TEST SECTION OPERATING WITHOUT SHOCK.

Flow is assumed to be isentropic to the nozzle throat and adiabatic thereafter. For ease of calculations, the nozzle contour as given in Figure 19a was assumed to consist of five straight line segments as listed in Table X.

Utilizing the influence coefficients of table 8.2 (2) multiplied by M^2 and designating the product F as outlined by Shapiro (2) for the combined effects of area change and friction results in the following equation

$$dM^2 = F_A \frac{DA}{A} + F_f \overline{4f} \frac{dx}{D}.$$

The technique of isoclines as given in Chapter 8 of Shapiro (2) was the means of arriving at a solution to this differential equation.

The parameters of the area A and the hydraulic diameter D may be expressed in terms of the tunnel dimensions. Area of the tunnel at any point is the product of the tunnel width w and the tunnel height h at the point in question. As the tunnel is of constant width, the area at any point is proportional to the height at that point and the derivative of the area proportional to the derivative of the tunnel height. The hydraulic diameter is defined as 4 times the area divided by the wetted perimeter and expressed in

tunnel dimensions is

$$D = \frac{4 \times \text{area}}{\text{wetted perimeter}} = \frac{4\,w\,h}{2\,(w+h)} = 2\,\frac{w\,h}{w+h}\,.$$

As the tunnel width w is constant throughout the length of the tunnel at 0.500 inches the hydraulic diameter may be expressed

$$D = 2\frac{(0.500)\,h}{0.500+h} = \frac{2\,h}{1+2h}\,.$$

As assumed, the nozzle segment heights will vary linearly in accordance with the equation for a straight line $h = mx + h_o$ where m is the slope of the nozzle segment at some distance x downstream of the nozzle throat and the nozzle throat having an initial height of h_o.

$$h = mx + h_o$$

$$dh = m\,dx \quad ; \quad dx = \frac{dh}{m}$$

at $x = L$, $h = h_1$ so the slope $m = \frac{h_1 - h_o}{L}$.

Combining these relationships and substituting them into the original differential equation

$$dM^2 = F_A\,\frac{dh}{h} + F_f(\overline{4f})\,\frac{L\,(w+h)}{2\,w\,h\,(h_1 - h_o)}\,dh$$

$$dM^2 = \frac{F_A}{h} + \frac{F_f(\overline{4f})\,L}{2\,w\,(h_1 - h_o)}\,\left(1 + \frac{w}{h}\right)\,dh$$

$$\frac{dM^2}{dh} = \frac{F_A}{h} + \frac{F_f(\overline{4f})\,L}{2\,w\,(h_1 - h_o)}\,\left(1 + \frac{w}{h}\right)$$

The equation is now in the form so that by suitable numerical values of h and M being substituted, the slope of the

Mach number squared is obtained. Values of h_1 are assumed in addition to values of M that are thought to bracket the actual Mach number. On a plot of M^2 vs. h, the calculated values of the slope dM^2/dh are plotted at the coordinate points of each assumed value of M and h. Sufficiently small increments of h must be utilized to provide the necessary isoclinic field. A smooth curve, starting tangent to be the value of dM^2/dh at the known value of h_o and its corresponding value of M is then drawn through the field of isoclines tangent to a reference isocline at each value of h the curve passes through. In addition to the physical data listed in the previous table a value of the average friction factor $(\overline{4f})$ equaling 0.01 was assumed with an initial Mach number of 1.00 existing in the nozzle throat.

A value of M^2 is determined from the junction of the smooth curve and the height at the segment end point. This calculated Mach number is then used as the initial Mach number for the second nozzle segment. Continuation of this process resulted in the adiabatic Mach number at the nozzle exit. Sample calculations for segment 2 are given in tabular form in Table XII and are plotted on figure 20.

Straightforward use of Table 42(3) for Fanno line procedure was used to predict the resultant Mach number at the end of the constant area section of the tunnel. Isoclinic procedures could have been used but this method was discarded as being time consuming compared to the use of the tables. The following information was assumed or

utilized for determining the exit Mach number:

$\overline{4f}$ = 0.01 and constant in value throughout the section

L = 5.75 inches, the tunnel section length

D = 0.775 inches, the hydraulic diameter

M_1 = Mach number at the nozzle exit equal 2.17

M_2 = Mach number at the section exit

Entering Table 42(3) with M_1 of 2.17, a value of $\overline{4f}L_{max}/D$ was read as 0.35298 for use in the following equation:

$$\left(\overline{4f}\,\frac{L}{D}\right)_{M_2} = \left(\overline{4f}\,\frac{L_{max}}{D}\right)_{M_1} - \left(\overline{4f}\,\frac{L_{max}}{D}\right)_{M_2}$$

$$\left(\frac{(\overline{4f}L_{max})}{D}\right)_{M_2} = \left(\frac{(\overline{4f}L_{max})}{D}\right)_{M_1} - \left(\frac{\overline{4f}L}{D}\right)_2$$

$$= 0.35298 - \frac{(0.01)\ (5.75)}{0.775} = 0.27878$$

Table 42(3) was then entered using this value of $\overline{4f}L/D$ and the Mach number at the end of the test section determined as 1.914.

PREDICTION OF ADIABATIC MACH NUMBER WITH A NORMAL SHOCK STANDING IN THE TUNNEL NOZZLE.

Flow was assumed to be adiabatic in the nozzle until the normal shock occurred at a point midway between pressure taps 4 and 5. M_x the Mach number upstream of the normal shock was determined as 2.0 as read from figure 20, which is a plot of the adiabatic Mach numbers as calculated

vs. tunnel length based on previous calculations in this appendix. Entering Table 48(3) with this value of M_x, the Mach number M_y downstream of the normal shock was obtained as 0.57735. M_y thus obtained was used as the initial value of M for the isocline technique for determining Mach numbers for points downstream of the normal shock in the nozzle and in the constant area section of the tunnel. The nozzle area and the corresponding nozzle height were read from figure 19a at the shock location assumed to be between pressure taps 4 and 5. Nozzle height at the assumed shock location is 1.30 inches.

As before, the remaining portion downstream of the shock in the diverging nozzle was assumed to consist of the same straight line segments. The initial section was taken as the remaining portion of the original segment 2 and was designated as segment 2a. All previous assumptions concerning the average friction factor and the physical data remained constant as outlined in Table XI.

A nozzle exit Mach number was found to be 0.429. The relationship of $\overline{4}fL/D$ at the inlet and exit of the constant area section was utilized to determine the Mach number at the end of the constant area section as was done in previous calculations in this appendix. This exit Mach number was found to be $M = 0.434$.

Theoretical values of P/P_{o1} at any point downstream of the shock are obtained by multiplying the value of P/P_o corresponding to the Mach number at that point by the value

of P_{oy}/P_{ox} obtained from Table 48 (3) for the Mach number at which the shock occurred. Based on the data in Table IX, it was assumed the shock occurred at a Mach number of 2.000 with P_{oy}/P_{ox} having a value of 0.7208. Adiabatic Mach numbers and pressure ratios obtained by this procedure are presented graphically in Figures 22 and 23.

Table XVI is a summary of the adiabatic Mach numbers predicted for the tunnel operating with and without a normal shock standing in the tunnel nozzle with a constant area section.

TABLE XVI - Summary of Adiabatic Mach Numbers in Nozzle

Pressure tap	Adiabatic Mach Number No Shock	Adiabatic Mach Number Shock in Nozzle
2	1.355	1.355
5	2.070	0.529
7	2.180	0.432
9	2.195	0.429
12	2.170	0.429
32 (end of constant area section)	1.914	0.434

DETERMINATION OF DIFFUSER HEIGHT TO PRODUCE CONSTANT MACH NUMBER IN TEST SECTION INCLUDING EFFECT OF FRICTION.

Assume that the diffuser height will increase linearly. Point t is taken as the nozzle throat; point 2, the end of the nozzle; and point 3 the maximum diffuser height location.

Utilizing the influence coefficients for constant specific heat and molecular weight from Shapiro's Table 8.2 [2]

$$\frac{dM^2}{M^2} = \frac{2\left(1+\frac{k-1}{2}M^2\right)}{1-M^2}\frac{dA}{A} + \frac{kM^2\left(1+\frac{k-1}{2}M^2\right)}{1-M^2}\frac{\overline{4f}\,dx}{D} = 0$$

$$2\frac{dA}{A} = \overline{4f}\,kM^2\frac{dx}{D}$$

Area of tunnel = width x height = w h and as tunnel is of constant width

$$dA \approx dh \quad \text{and} \quad \frac{dA}{A} \approx \frac{dh}{h}$$

The hydraulic diameter $D = \frac{4\ (\text{area})}{\text{Wetted perimeter}} = \frac{4\ w\ h}{2\ (w+h)} = \frac{2\ w\ h}{w+h}$. Substituting the values

$$2\frac{dA}{A} = 2\frac{dh}{h} = \frac{\overline{4f}\,kM^2dx}{2wh}(w+h)$$

Combining terms

$$\frac{4w\,dh}{w+h} = 4\bar{f}k M^2 dx$$

$$w\int_{h_2}^{h_3} \frac{dh}{w+h} = \bar{f}kM^2 \int_{x_2}^{x_3} dx$$

Integrating between designated limits

$$w\ln(w+h)\Big]_{h_2}^{h_3} = kM^2\bar{f}(X_3 - X_2)$$

$$\ln\left(\frac{w+h_3}{w+h_2}\right) = \frac{kM^2\bar{f}(X_3 - X_2)}{w}$$

clearing and solving for h_3

$$h_3 = -w + (w+h)e^{\frac{kM^2\bar{f}(X_3 - X_2)}{w}}$$

Substituting values of w = 0.5 inches; h_2 = 1.718 inch; M_2 = 2.17; $X_3 - X_2$ = 5.33 inches, Figure 20.

$$h_3 = 0.5 + (2.218)e^{\frac{4(2.17)^2(0.0025)(5.33)}{0.5}}$$

$$h_3 = 0.5 + 2.645 = 2.145 \text{ inches.}$$

The maximum theoretical height of the diffuser to obtain a constant adiabatic Mach number of 2.17 could not be obtained in the diffuser section due to physical limitations of the tunnel itself. As may be noted in Figure 19b,

the diffuser contours actually existing are far from the theoretical solution of the maximum diffuser height. The actual contour required is of an exponential nature as developed previously. Values required in the diffuser to produce a constant adiabatic Mach number in the diffuser vs. diffuser length are presented in Table XIII in tabular form and plotted in Figure 19b. Numerical values of x were inserted in the exponential equation derived for determining the diffuser height.

DETERMINATION OF MINIMUM DIFFUSER AREA TO ALLOW SUPERSONIC FLOW.

As in the case of the diverging nozzle, it was assumed the diffuser converged linearly from the maximum nozzle exit height of 1.718 inches to some minimum height less than 1.718 inches. The same isoclinic technique was employed to determine this minimum height and allow supersonic flow to exist. The most severe condition that may be encountered is to have a normal shock at the nozzle exit or at some other location upstream of the diffuser throat. This condition will exist upon the initial start of the tunnel blow. The minimum diffuser height must be sufficiently large to pass the given mass rate of flow in the subsonic condition. Assuming a normal shock occurring at the nozzle exit, with a Mach number of 2.17 existing in the nozzle exit, the initial Mach number for the diffuser will be 0.551 as taken from the Gas Tables (3) for normal isentropic shock. At the minimum area, the Mach number must increase to 1.00.

Various values of the minimum diffuser height h are assumed, the isoclinic field drawn for these conditions and the smooth curve faired through the isoclinic field. Various values of h, the minimum diffuser height, had to be assumed to meet the end point conditions, namely, the curve had to have an infinite slope at the junction of h and the Mach number squared equaling one. Table XIV presents the data for determining the minimum height in tabular form and Figure 2-F is a plot of the isoclinic field for a minimum diffuser height of 1.40 inches. All isoclines are not plotted to reduce the clutter near the terminal point of the curves. The slope of dM^2/dh changes radically near the terminal point requiring a large number of isoclines to be plotted.

DETERMINATION OF MACH NUMBER AT DIFFUSER THROAT WITH DIFFUSER HEIGHT = 1.40 INCHES CONSIDERING FRICTION

Conditions at nozzle throat are designated by t, at the nozzle exit by 2, and at the diffuser throat by 3.

Utilizing the influence coefficients of Table 8.2 multiplied by M^2 and designating the product F as outlined by Shapiro [2] for the combined effects of area change and friction

$$dM^2 = F_A \frac{dA}{A} + F_f 4\bar{f} \frac{dx}{D}$$

Area of tunnel = width x height = wh

As A $\propto$ h for constant width tunnel

$$dM^2 = F_A \frac{dh}{h} + F_f \overline{4f} \frac{dx}{D}$$

hydraulic diameter $D = \frac{4 \times \text{area}}{\text{Wetted perimeter}} = \frac{4\ wh}{2(w+h)} = 2\frac{wh}{w+h}$

$w = \frac{1}{2}$ inch

$$D = \frac{2(1/2)h}{1/2+h} = \frac{2h}{1+2h}$$

Substituting this value of $1/D$

$$dM^2 = F_A \frac{dh}{h} + \frac{F_f \overline{4f}\, dx}{2h} + F_f \overline{4f}\, dx$$

Assume that the diffuser height will vary linearly in accordance with the relationship

$$h = mx + h_o$$

where m is the slope of the diffuser and x is the distance down the tunnel.

At

$x = x_2 = 4.802$ inches, $h = h_2 = 1.718$ inches,

and at

$x = 10.8$ inches, $h = h_3 = 1.40$ inches

$$m = \frac{h_3 - h_2}{x_3 - x_2} = \frac{1.4 - 1.718}{10.8 - 4.8} = -0.0530$$

$$dh = m\,dx \; ; \; dx = \frac{dh}{m}$$

$$dM^2 = \left[\frac{F_o}{h} + \frac{\overline{4f}\, F_f}{2hm} + \frac{\overline{4f}\, F_f}{m}\right] dh$$

Let

$$\bar{h} = \frac{h_3 + h_2}{2}$$

and

$$\bar{M} = \frac{M_2 + M_3}{2} \qquad \text{for determination of } \bar{F}$$

$$\bar{h} = \frac{1.718'' + 1.4''}{2} = 1.559 \text{ inches}$$

$$\bar{f} = 0.0025$$

$$M_2 = 2.17 \qquad \text{from Figure 20}$$

$$M_3^2 - M_2^2 = \left[\frac{1}{\bar{h}} F_A + \frac{4\bar{f}\,\bar{F}_f}{m}\left(\frac{1}{2\bar{h}} + 1\right)\right](h_3 - h_2)$$

$$M_3^2 - M_2^2 = \left[\frac{1}{1.559} F_A + \frac{4(0.0025)}{-0.0530}\left(\frac{1}{3.118} + 1\right)\bar{F}_f\right](1.4 - 1.718)$$

$$M_3^2 - M_2^2 = -0.221\,\bar{F}_A + 0.0792\,\bar{F}_f$$

Assuming a value of M_3 to determine $\bar{M}$ and the values of the influence coefficients from Table B-6 [2], a process

of iteration may be made to find the correct value of M_3

Try $M_3 = 1.63$; $\bar{M} = \frac{1.63 + 2.17}{2} = 1.90$

$$\bar{F}_A = 4.7635$$
$$\bar{F}_f = -12.038$$

$$M_3^2 - M_2^2 = -0.221\bar{F}_A + 0.0792\bar{F}_f$$

$$M_3^2 = 4.70 - 0.221(4.7635) - 0.0792(12.038)$$

$$M_3^2 = 2.70$$
$$M_3 = 1.642$$

Try $M_3 = 1.64$; $\bar{M} = 1.905$

$$\bar{F}_A = 4.7649$$
$$\bar{F}_f = -12.106$$

$$M_3^2 = 4.70 - 0.221(4.7649) - 0.0792(12.106)$$

$$M_3^2 = 2.69$$
$$M_3 = 1.64$$

In addition to the analytical solution for determining the Mach number at the diffuser throat, an isoclinic field plot was drawn and an exit Mach number obtained by this technique. The Mach number as determined by the use of isoclines was 1.71 compared to a Mach number of 1.64 as determined by the analytical solution. Table XV and Figure 3-F present the information necessary to plot the isoclinic field and a plot of the field itself.

DETERMINATION OF EXPERIMENTAL ADIABATIC MACH NUMBERS FOR SHOCK FREE CONDITIONS

Assume that flow to the nozzle throat is isentropic and that the flow for the remainder of the tunnel system is adiabatic. From the Gas Tables for isentropic flow (3) the adiabatic Mach number, M, at any desired point may be determined for shock free flow conditions under the product

$$\left(\frac{A}{A^*}\right)\left(\frac{P}{P_o}\right)$$

providing A^* and P_o are taken as the area and stagnation pressure when the Mach number is unity. $P/P_o = 1 - \frac{\Delta P}{P_o}$ with pressures P_o and ΔP being measured by the use of manometers. Consider pressure tap 16 at the outlet of the nozzle as station 1 and tap 31 in the diffuser as station 2.

Data is taken from Table V or Figure 20 for a shock free run with the diffuser set at a constant height of 1.718 inches.

$$(A/A_x^*) = 2.34$$

$$(P/P_o)_1 = 0.0844$$

$$(A/A_x^*)\ (P/P_o)_1 = 2.34 \times .0844 = 0.1975$$

From the Gas Tables for isentropic flow (3) using the above value for entering the tables M_1 is determined as being 2.125. All adiabatic Mach numbers upstream of a shock were determined in this manner.

DETERMINATION OF EXPERIMENTAL ADIABATIC MACH NUMBERS FOR SHOCK IN NOZZLE OPERATION.

The adiabatic Mach number for points downstream of the shock in the nozzle are determined in the same manner as for shock free conditions. Taking data from Table IX for pressure tap number 20, the product $(A/A_x^*)\ (P/P_o)_1$ was calculated as being 0.941. Entering Table 30 (3) with this value, the adiabatic Mach number was determined as being 0.594. The ratio of change in stagnation pressure at pressure tap 20 or at any other location downstream of the shock in the tunnel to the initial stagnation pressure is obtained by the relation

$$\left(\frac{P_{oy}}{P_{o1}}\right)_n = \left(\frac{P}{P_{o1}}\right)\left(\frac{P_{oy}}{P}\right)_n$$

The value of $(P/P_{oy})_n$ being evaluated from table 30 (3) at the Mach number M_n under the column P/P_o.

DETERMINATION OF EXPERIMENTAL MEAN FRICTION COEFFICIENT

To eliminate as many variables as possible, data with the diffuser set at a constant height of 1.718 inches and the tunnel running shock free was used, i.e., Fanno Flow.

With the value of M having been determined from data in Table V as being 2.125, at point 1, the constant area inlet, this Mach number was used as the argument to enter the Gas Tables (3) for Fanno Flow and evaluate the following:

$$\left(\frac{P}{P^*}\right)_1 = 0.3737$$

$$\left(\frac{4\bar{f}L_{max}}{D}\right)_1 = 0.3407$$

Now since

$$\frac{P_2}{P_1} = \frac{(P/P^*)_2}{(P/P^*)_1}$$

we obtain

$$\left(\frac{P}{P^*}\right)_2 = \frac{0.1088}{0.844}(0.3737)$$

$$= 0.481$$

From the Gas Tables (3) for the Fanno Line flow using $(P/P^*)_2 = 0.481$ the Mach number at the constant area pressure tap 31, point 2, is determined as being 1.78 and

the corresponding value of $\left(\frac{\overline{4f}L_{max}}{D}\right)_2$ as 0.23520

$$\left(\frac{\overline{4f}\,\Delta L}{D}\right)_1 = 0.3737 - 0.2350 = 0.1385$$

$$D = 0.775 \text{ inches}$$

$$\Delta L = 10.00'' - 4.75'' = 5.25 \text{ inches}$$

$$\overline{4f} = \frac{0.1358 \times 0.775}{5.25}$$

$$= 0.01865$$

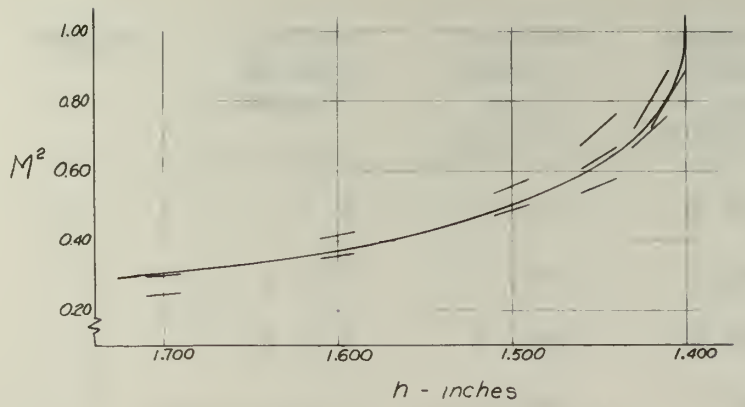

Figure 2-F. Isoclinic Field for Determioetion of the Minimum Diffuser Height for Supersonic Operetion.

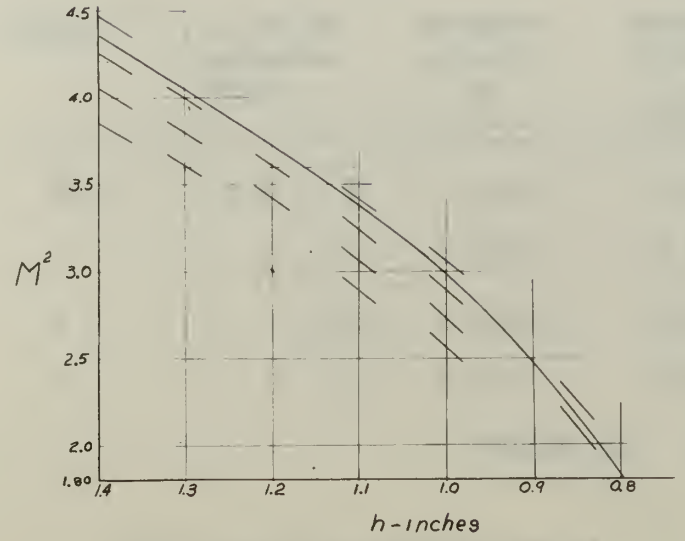

Figure 1-F. Isocliotc Field for Determioetion of the Mach Number at Exit of Segment Two of Nozzle While Operetiog Shock Free.

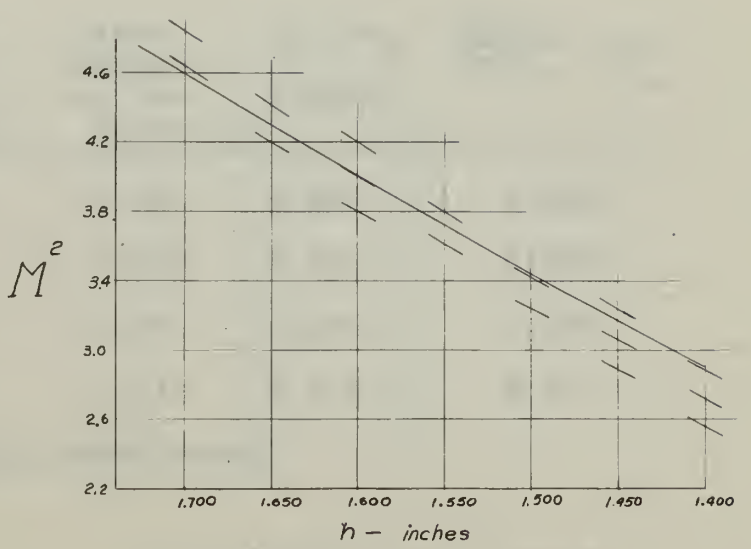

Figure 3-F. Isoclinic Field for Determinetion of the Mach Number at the Mioimum Diffuser Area.

Segment	Located Between Taps	Segment Length in Inches	Segment Width in Inches	Initial Height h_o in Inches	Final Height h_1 in Inches	$h_1 - h_o$ Inches	$\frac{\bar{4}fL}{2w(h_1 - h_o)}$
1	1 - 2	0.50	0.500	0.734	0.804	0.070	0.715
2	2 - 5	1.500	0.500	0.804	1.382	0.578	0.0259
3	5 - 7	1.000	0.500	1.382	1.608	0.226	0.0443
4	7 - 9	1.000	0.500	1.608	1.700	0.092	0.108
5	9 - 12	0.750	0.500	1.700	1.718	0.018	0.417

TABLE X. Simplified Nozzle Coordinates

Segment	Located Between Taps	Segment Length in Inches	Segment Width in Inches	Initial Height h_o in Inches	Final Height h_1 in Inches	$h_1 - h_o$ Inches	$\frac{\bar{4}fL}{2w(h_1 - h_o)}$
2a	4.5 - 5	0.250	0.500	1.300	1.382	0.082	0.0305
3	5 - 7	1.000	0.500	1.382	1.608	0.226	0.0443
4	7 - 9	1.000	0.500	1.608	1.700	0.092	0.108
5	9 - 12	0.750	0.500	1.700	1.718	0.018	0.417

TABLE XI. Simplified Nozzle Coordinates

TABLE XII. Data for Isoclinic Determination of Adiabatic Mach Number in Segment Two of Nozzle Operating Shock Free

h	M	M^2	F_A	F_f	$1 \frac{w}{h}$	K_1	K_2	$\frac{dM^2}{dh}$
0.804	1.355	1.8400	5.9910	-7.7250	1.622	7.4600	-0.3250	7.134
0.810	1.350	1.8225	6.0469	-7.7144	1.618	7.4600	-0.3235	7.137
	1.400	1.9600	5.6840	-7.7984		7.0000	-0.3230	6.697
0.850	1.400	1.9600	5.6840	-7.7984	1.588	6.6800	-0.3210	5.938
	1.450	2.1025	5.4179	-7.9738		6.3800	-0.3275	5.053
	1.500	2.2500	5.2200	-8.2215		6.1400	0.3380	5.802
0.900	1.450	2.1025	5.4179	-7.9738	1.556	6.0200	-0.3215	5.699
	1.500	2.2500	5.2200	-8.2215		5.7800	-0.3320	5.448
	1.550	2.4025	5.0722	-8.5302		5.6200	-0.3440	5.276
0.950	1.500	2.2500	5.2200	-8.2215	1.527	5.4700	-0.325	5.145
	1.550	2.4025	5.0722	-8.5302		5.3200	-0.337	4.983
1.000	1.600	2.5600	4.9625	-8.8927	1.500	4.9625	-0.345	4.617
	1.650	2.7225	4.8823	-9.3045		4.8823	-0.362	4.521
	1.700	2.8900	4.8258	-9.7627		4.8260	-0.380	4.446
1.050	1.600	2.5600	4.9625	-8.8927	1.476	4.7200	-0.340	4.380
	1.650	2.7225	4.8823	-9.3045		4.6500	-0.356	4.294

TABLE XII - Cont'd

h	M	M^2	F_A	F_f	$1 \frac{w}{h}$	K_1	K_2	$\frac{dM^2}{dh}$
1.10	1.70	2.8900	4.8258	- 9.7627	1.455	4.380	-0.368	4.012
	1.75	3.0625	4.7886	-10.266		4.340	-0.387	3.953
	1.80	3.2400	4.7674	-10.812		4.330	-0.408	3.922
	1.85	3.4225	4.7597	-11.403		4.325	-0.432	3.893
1.15	1.75	3.0625	4.7886	-10.266	1.435	4.080	-0.381	3.699
	1.80	3.2400	4.7674	-10.812		4.140	-0.402	3.738
1.20	1.85	3.4225	4.7597	-11.403	1.417	3.960	-0.420	3.540
	1.90	3.6100	4.7635	-12.038		3.970	-0.447	3.528
	1.95							
1.25	1.85	3.4225	4.7597	-11.403	1.400	3.800	-0.414	3.386
	1.90	3.6100	4.7635	-12.038		3.815	-0.437	3.378
1.30	1.90	3.6100	4.7635	-12.038	1.385	3.670	-0.432	3.238
	2.00	4.0000	4.8000	-13.440		3.700	-0.483	3.227
	1.95	3.8025	4.7774	-12.716		3.670	-0.452	3.218
	1.85	3.4225	4.7597	-11.403		3.665	-0.410	3.255

TABLE XII - Cont'd

h	M	M^2	F_A	F_f	$1 \frac{w}{h}$	K_1	K_2	$\frac{dM^2}{dh}$
1.382	1.95	3.8025	4.7774	-12.716	1.362	3.450	-0.449	3.001
	2.00	4.0000	4.8000	-13.440		3.470	-0.476	2.994
	2.05	4.2025	4.8305	-14.210		3.495	-0.525	2.970
	2.10	4.4100	4.8678	-15.027		3.520	-0.530	2.990
	2.15	4.6225	4.9115	-15.892		3.560	-0.562	2.998
	2.20	4.8400	4.9610	-16.808		3.590	-0.595	2.995

TABLE XIII.

Diffuser Contours Required to Produce a Constant Mach Number

Diffuser Length Inches	Diffuser Height Inches
0.000	1.718
0.500	1.755
0.750	1.755
1.000	1.795
1.250	1.815
1.500	1.830
1.750	1.845
2.000	1.865
2.250	1.885
2.500	1.905
2.750	1.925
3.000	1.950
3.250	1.970
3.500	1.990
3.750	2.010
4.000	2.030
4.250	2.050
4.500	2.075
4.750	2.095
5.000	2.110
5.250	2.135
5.330	2.145

TABLE XIV. Isocline Data for Determination of Minimum Diffuser Area

h	M	M_2	F_A	F_f	$1 \frac{w}{h}$	K_1	K_2	$\frac{dM^2}{dh}$
1.718	0.551	0.3036	-0.9485	0.20570	1.291	-0.552	-0.045	-0.597
1.700	0.500	0.2500	-0.7000	0.12250	1.294	-0.412	-0.027	-0.439
	0.550	0.3025	-0.9199	0.19478		-0.541	-0.042	-0.583
	0.600							
1.650	0.550	0.3025	-0.9199	0.19478	1.303	-0.557	-0.043	-0.600
	0.600	0.3600	-1.2060	0.30391		-0.730	-0.066	-0.796
1.600	0.600	0.3600	-1.2060	0.30391	1.312	-0.754	-0.067	-0.821
	0.650	0.4225	-1.5868	0.46931		-0.992	-0.103	-1.095
1.550	0.650	0.4225	-1.5868	0.46931	1.323	-1.023	-0.104	-1.127
	0.700	0.4900	-2.1099	0.72369		-1.360	-0.160	-1.420
1.500	0.700	0.4900	-2.1099	0.72369	1.333	-1.409	-0.162	-1.571
	0.750	0.5625	-2.8607	1.12640		-1.909	-0.251	-2.160
	0.800	0.6400	-4.0107	1.79680		-2.680	-0.400	-3.080
1.450	0.750	0.5625	-2.8607	1.12640	1.345	-1.971	-0.254	-2.225
	0.800	0.6400	-4.0107	1.79680		-2.770	-0.405	-3.175
	0.850	0.7225	-5.9596	3.01410		-4.110	-0.679	-4.789

TABLE XIV, Cont'd

h	M	M_2	F_A	F_f	$1 \frac{w}{h}$	K_1	K_2	$\frac{dM^2}{dh}$
1.420	0.800	0.6400	-4.0107	1.7968	1.352	-2.830	-0.406	-3.236
	0.850	0.7225	-5.9596	3.0141		-4.200	-0.683	-4.883
	0.900	0.8100	-9.9076	5.6176		-6.980	-1.273	-8.253
	0.950	0.9025	-21.8540	13.8060		-15.400	-3.120	-18.520
1.410	0.900	0.8100	-9.9076	5.6176	1.354	-7.030	-1.270	-8.300
	0.950	0.9025	-21.8540	13.8060		-15.510	-3.130	-18.640
1.400	0.850	0.7225	-5.9596	3.0141	1.357	-4.260	-0.685	-4.945
	0.900	0.8100	-9.9076	5.6176		-7.080	-1.277	-8.357
	0.950	0.9025	-21.8540	13.8060		-15.600	-3.140	-18.740
	1.000	1.0000						

TABLE XV. Determination of Mach Number at Minimum Area Conditions by Isoclines

h	M	M^2	F_A	F_f	$1 \frac{w}{h}$	K_1	K_2	$\frac{dM^2}{dh}$
1.718	2.17	4.7000	4.9313	-16.258	1.291	2.87	3.52	6.39
1.700	2.20	4.8400	4.9610	-16.808	1.294	2.92	3.55	6.47
	2.15	4.6225	4.9115	-15.892		2.89	3.44	6.33
	2.10							
1.650	2.10	4.4100	4.8678	-15.027	1.303	2.95	3.29	6.24
	2.05	4.2050	4.8305	-14.210		2.93	3.11	6.04
	2.00							
1.600	2.05	4.2050	4.8305	-14.210	1.312	3.01	3.13	6.14
	2.00	4.0000	4.8000	-13.440		3.00	2.96	5.96
	1.95	3.8025	4.7740	-12.716		2.98	2.80	5.78
1.550	1.95	3.8025	4.7740	-12.716	1.323	3.08	2.82	5.90
	1.90	3.6100	4.7635	-12.038		3.07	2.67	5.74
1.500	1.85	3.4225	4.7597	-11.403	1.333	3.18	2.55	5.73
	1.80	3.2400	4.7674	-10.812		3.18	2.42	5.60

TABLE XV - Cont'd

h	M	M^2	F_A	F_f	$1 \frac{w}{h}$	K_1	K_2	$\frac{dM^2}{dh}$
1.450	1.75	3.0625	4.7886	-10.266	1.345	3.30	2.31	5.61
	1.70	2.8900	4.8258	-9.763		3.33	2.10	5.43
	1.80	3.2400	4.7674	-10.812		3.29	2.41	5.70
1.400	1.70	2.8900	4.8258	-9.763	1.357	3.45	2.22	5.67
	1.65	2.7225	4.8823	-0.305		3.48	2.11	5.59
	1.60	2.5600	4.9625	-8.893		3.55	2.02	5.57

APPENDIX G

AIR RECEIVER CAPACITANCE DESIGN CALCULATIONS AND PREDICTED TEMPERATURE VARIATIONS

To maintain an isothermal blowdown, Muto [15] states the ratio (1), $C_o^* = \frac{M_c C_p}{M_b C_v}$ should have as a minimum value of 7.5, and the non dimensional number of transfer units (2), NTU $= \frac{hA}{C_v \dot{m}}$ should have a minimum value of 7.5.

Storage tank dimensions

48 in. Outside Diam

11 ft. 4 in. height

.75 in. heads

.781 in. shells

Mass in tanks = M_c lbm.

$$= 2\rho_{metal}\left[\pi d t l + \frac{2\pi d^2 t}{4}\right]$$

$$= 2\rho_{STEEL}\left[\frac{\pi \times 47.22 \times 0.781 \times 136 + \frac{\pi(47.22)}{2} \times 0.75}{1728}\right]$$

$$M_c = 10{,}410 \text{ lb mass of steel.}$$

Surface Area of tanks

$$= 2\left[\pi d_{inside} l + \frac{2\pi d_{inside}^2}{4}\right] =$$

$$= 2\left[\frac{\pi(46.44)136 + \frac{\pi(46.44)^2}{2}}{144}\right]$$

$$\text{AREA} = 183.5 \text{ square feet.}$$

Mass of air initially in tank as beginning of blowdown = Mb

Initial tank pressure = 475 Psia.

$$Mb = \frac{PV}{RT} = \frac{475\ \#/in^2 \times 144\ in^2/ft^2 \times 2\ tanks \times 177\ ft^3/tank}{53.34\ \frac{ft-\#}{lbm-^\circ R} \times 520^\circ R}$$

Mb = 577 lbm. air initially in tank.

Mass of air in tanks at end of blowdown at 150 psia

$$Me = 577\ \frac{150}{475} = 182\ lb_m\ @\ 150\ psia$$

$$M^* = \frac{Me}{M_b} = 182/577 = 0.31$$

Substituting the above values into equations 1 and 2

$$C_o^* = \frac{M_c\ C_{p\ STEEL}}{M_b\ C_v} = \frac{10,410 \times 0.113}{577 \times 0.173} = 11.8$$

using a value of h = $3\ \frac{BTU}{hr\ ft^2\ ^\circ R}$ and $\dot{m} \approx 1100\ lbm/hr$

$$NTU = \frac{h\ A}{C_v\ \dot{m}} = \frac{3 \times 183.5}{0.173 \times 1100}$$

NTU = 2.89

Since the value of $C_o^* > 7.5$ and the value of NTU < 7.5 the value of NTU must be increased by increasing the area available for the heat transfer

$$NTU = 7.5 = \frac{h\ A}{C_v\ \dot{m}}$$

$$A = \frac{7.5 \times 0.173 \times 1100}{3} = 476\ ft^2$$

additional area required

$$476\ ft^2 - 183.5\ ft^2 = 292.5\ ft^2.$$

if 1/8 inch aluminum sheet is used to reduce to corrosion problem, the mass of aluminum required utilizing both sides of sheet for heat transfer

$$\text{Mass Al} = \rho_{AL}\left[\frac{292.5\ ft^2}{2} \times \frac{0.125}{12}\ ft\right] = 169\ \frac{lbm}{ft^3}\left[1.525\ ft^3\right]$$

Mass Al = 257 lbm.

Utilizing eqn 9A as developed by Muto [15] to predict the storage tank air temperature after a blow down with the presently installed tanks without additional corrective heating surfaces and comparing this value to the temperature actually noted after a blowdown very close correlation was noted.

Eqn 9A by Muto to predict temp after blow

$$T^* = \frac{T}{T_o} = \left(\frac{M^* + C_o^*}{1 + C_o}\right)^{.4} = \left(\frac{0.31 + 11.8}{1 + 11.8}\right)^{.4}$$

$T^* = 0.9785$

with To = 523°R from Figure 1-G

Tend of blow = 0.9785 x 523°R = 511°R

From Figure 1-G, actual temperature of the storage tank air at the end of a 10 minute run = 510.5°R.

FIG 1-6 DECREASE OF STAGNATION TEMPERATURE VS. TIME OF TUNNEL OPERATION

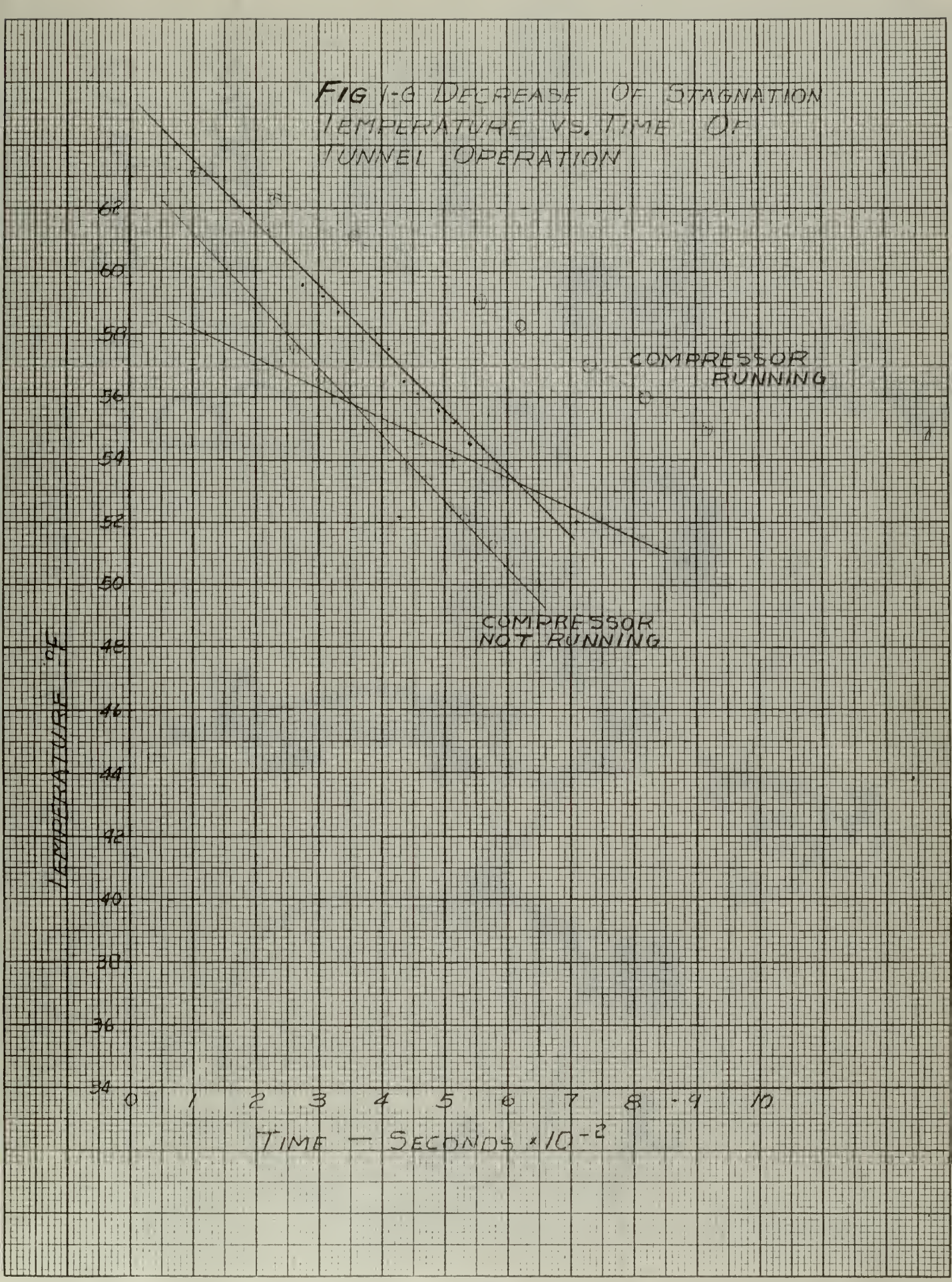

YOU TOO, ARE INVITED TO

CHARLIE BROWN'S

BLOW-DOWN

FRIDAY
AFTERNOON
APRIL 1ST

GOOD GRIEF!
WHAT BETTER
DAY?